A molecular dynamics study of Hras-GTP complex and Hras-GDP complex

Takeshi MIYAKAWA

Division of Mathematical and Physical Science,

Graduate School of Natural Science and Technology,

Kanazawa University

2012

Acknowledgment

The doctoral thesis is a summary of my study from October 2009 to July 2012 at the Division of Mathematical and Physical Science, Graduate School of Natural Science and Technology of Kanazawa University.

I am very grateful to Professor Hidemi Nagao for fruitful discussions and encouragement of the study. I am very grateful to Professor Masako Takasu at Tokyo University of Pharmacy and Life Sciences for various discussions and advice. I would like to thank Professor Mineo Saito, Professor Tatsuki Oda, Professor Shinichi Miura, Dr. Hiroaki Saito and Dr. Kazutomo Kawaguchi at Kanazawa University, Dr. Ryota Morikawa at Tokyo University of Pharmacy and Life Sciences, Dr. Kimikazu Sugimori at Kinjo University, Dr. Shuhei Kawamoto at National Institute of Advanced Industrial Science and Technology, Professor Tetsuta Kato, Professor Yasuhiko Yamada, Professor Akira Dobashi, and all colleagues at Tokyo University of Pharmacy

and Life Sciences for their advice and their supports. I also would like to thank all students at the computational biophysics group of Kanazawa University for their advice and their supports.

Lastly, I thank my families, friends and colleagues for enduring supports.

Contents

Chapter 1

Introduction

In this chapter, we explain the background and overview of this thesis.

1.1 Background

In this section, the background of this thesis is explained. The computer is powerful tool for investigating the problems of biology. We investigate the Hras protein, which plays an important role at signal transduction in the cell. The mutation of Hras protein is often observed in the tumor cell. *Hras* gene is considered as a proto-oncogene, which causes a canceration if the carcinogenic mutation occurs. So in this section, we explain the role of computers in 1.1.1, signal transduction in the cell in 1.1.2, proteins in 1.1.3

and cancers in 1.1.4. In 1.1.1–1.1.4, we use the description in Molecular Biology of the Cell 5th edition [1] as reference.

1.1.1 The role of computers in biology

In this subsection, we explain the role of computers in biology.

Aim of simulation

In only few cases, we can calculate analytically the physical properties of the system. In many cases, we can calculate analytically the physical properties using some approximations. When we use the approximations, we can hardly ascertain that the features of the results are caused by that approximations or by the real nature of that target system. The aim of simulation is calculating the physical properties of the target system using the generic approximations, such as discretization, numerical treatment instead of the specific approximations of the target system. The relation of target areas is summarized in the Fig. 1.1. Experimental study is limited by the experimental methods and the experimental equipment. Theoretical study is limited by the theories about the target system. Analytical study is limited by the approximations which make analytical approaches possible. Simulational study

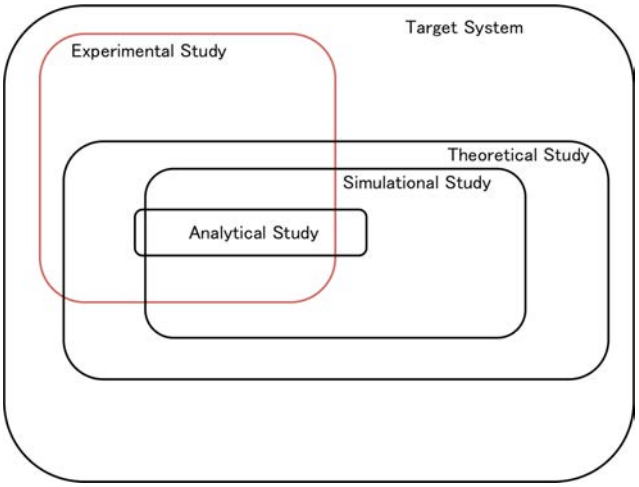

Figure 1.1: The relationship of target areas of experimental study and theoretical study. Theoretical study includes analytical study and simulational study.

is limited by the approximations which make simulations possible.

Molecular dynamics of proteins

The first MD simulations of rigid body spheres were performed in 1957 by B. J. Alder and T. E. Wainwright [2]. In 1964, A. Rahman performed the MD simulations of spherical molecules [3]. In 1971, A. Rahman and F. H. Stillinger performed the MD simulations about the rotation of water molecules [4]. In 1977, J-P. Ryckaert *et al.* published a paper about the SHAKE methods [5]. SHAKE is a constraint method on the bond length. In 1977, the MD simulations of the bovine pancreatic trypsin inhibitor (BPTI)

were performed in vacuum [6]. In 1980, H. C. Andersen performed the MD simulations of the constant pressure ensemble [7]. In 1981, M. Parrinello and A. Rahman performed the MD simulations of the constant pressure tensor ensemble [8]. In 1984, S. Nóse performed the MD simulations of the constant temperature ensemble [9]. In 1988, W. L. Jorgensen *et al.* published a paper about OPLS (Optimized Potentials for Liquid Simulations), which is one of the famous general purpose potential [10]. In 1991, M. Saito performed MD simulations of human lysozyme in solvent with good results [11].

How to treat implicitly the water

In the ordinary MD simulations of the protein system, the speed of simulations is limited by the calculation time of the water molecules. In order to perform the MD simulations of the protein system, we can use the "implicit" method, without treating the water molecules explicitly. Instead of this method, treating the water molecules explicitly is the main stream in the MD simulations of the protein system. Here, I explain the basis of the implicit method and mention the outline of the method. I survey the range of use and the limit of application of the implicit method.

The implicit methods describe the way in which the free energy of sol-

vation is calculated approximately. In the approximated method, the free energy is divided into two parts: the polar part and the non-polar part. The non-polar part is calculated using the fact that this part is proportional to the accessible surface area (ASA), and the polar part is calculated by the continuous dielectric model. The fact is well known that ASA is proportional to the free energy of transfer of the process in which the nonpolar amino acid is transferred from the water solvent to the organic solvent such as ethanol [12]. The fact was shown that ASA is also proportional to the free energy of transfer of the process in which the amino acid is transferred from the vacuum to the water solvent [13].

When the polar part is calculated by the continuous dielectric model, we use the approximation that the positions and the directions of the solvation molecules change immediately for a given protein conformation. This is based on the concept that the motion of the solvation molecules is much more rapid than the motion of the protein molecules. Integrating only the phase space of the motion of the solvent, the protein moves in the averaged solvent environment, that is the parameterized environment. In order to solve the problems in the continuous dielectric model, we need to solve the Poisson-Boltzmann equations. However, these equations can not be solved

analytically. One of the approximate method of solving these equations is Generalized Born (GB) model [14, 15] reviewed in [16]. The GB model has the advantage of shorter time for calculation, and also gives the force, which is the gradient of the potentials. The force is needed for the MD simulations.

The implicit method is called GB/SA method, because in this method both GB and SA are used. Here, I mention an instance showing the limit of the GB/SA method. Watanabe *et al.* calculated the free energy dependence on the reaction coordinate, which is the distance between the O_1 and the H_4 in the Ace-Ala-Ala-Nme peptide in the water solvent, using both the method with explicit water molecules and GB/SA method [17]. The GB/SA model does not account for the hydrogen bond effect between the peptide and explicit water molecules. The GB/SA model tends to overestimate the frequencies of the structures, which are stabilized by these intra-peptide hydrogen bonds.

The GB/SA method is appropriate for showing the capable structural model. However, the GB/SA method is not appropriate for the the quantitative calculations and not appropriate for the precise evaluation of the detail of the water molecules such as the hydrogen bond of the water molecules near the surface of the protein.

Molecular force field

Molecular model is based on the concept that the bond length, the bond angle and the dihedral angle in molecule are specified by the combination of atoms. Namely, the bond length, the bond angle and the dihedral angle in molecule do not depend much on the species but depend on the combination of atoms. A. W. von Hofman made the molecular model for the first time in 1860 [18]. J. H. van't Hoff made the three-dimensional model of ethane, ethylene and acetylene in 1874 [19].

Molecular force field is also based on the same concept as mentioned above: the two-body forces, three-body forces and four-body forces in molecule do not depend much on the species but depend on the combination of atoms. The basic concept of molecular force field is written by D. H. Andrews in 1930 [20]. F. H. Westheimer *et al.* applied the molecular force field to diphenyl using Born-Oppenheimer approximation in 1946 [21]. J. B. Hendrickson calculated the structure of cyclohexane using electronic computer in 1961 [22]. K. B. Wiberg optimized the structures using the steepest descent method in 1965 [23]. P. De Santis *et al.* applied the molecular force field to the study of structures of a macromolecular substance in 1963 [24]. D. A. Brant *et al.* applied the molecular force field to the study of structures of a

dipeptide in 1965 [25]. N. L. Allinger *et al.* applied the molecular force field to conformational analysis of hydrocarbons in 1971 [26].

The Born-Oppenheimer approximation is the approximation that we can separate the motion of electrons and the motion of nuclei. We can select the appropriate variables describing the relative positions of nuclei, and we can describe the potential energy by these variables. We use the following form of the potential V.

$$V = \sum_{i<j} E_{\mathrm{Bond}}(r_{ij}) + \sum_{i<j<k} E_{\mathrm{Angle}}(\theta_{ijk}) + \sum_{i<j<k<l} E_{\mathrm{Dihedral}}(\phi_{ijkl}) + \sum_{i<j} E_{\mathrm{NonBond}}(r_{ij}), \tag{1.1}$$

where E_{Bond} is caused by the bond length force, E_{Angle} is caused by the bond angle force, E_{Dihedral} is caused by the dihedral angle force, and E_{NonBond} is caused by the forces between not bonded atoms. In this thesis, we use the Amber force field describing in eq. (2.1).

In the above, we mentioned that the two-body forces, three-body forces and four-body forces in molecule do not depend much on the species but the combination of atoms. In fact, because the structures of molecules are different for the different electronic states even for the same species of atoms, molecular force fields are different for the different electronic states. For

molecular force field, we take into account these differences using atomic types describing the electronic states of atoms in molecules. Strictly speaking, the number of the atomic types is needed for the different molecules. However, for the realistic calculations, the number of the atomic types is from 20 to 30.

Using the molecular force field, we can estimate the stability of molecular structures, and this method is called molecular mechanics. We can also estimate the motion of the atoms in molecules with the equations of motion based on the molecular force field, and this method is typical molecular dynamics (MD).

Density Functional Theory (DFT)

The derivation of wave functions of electrons in molecules and atoms was performed just after the establishment of quantum mechanics. The wave functions could be derived analytically only for the rather simple system with high symmetry. Instead of wave function, the electron density was tried to explain the physical quantities of the electronic system in Thomas-Fermi-Dirac model in 1920s. In 1950s, Slater determinant was used to approximate the wave functions in many electronic systems. Based on these approaches, in

1960s, Hohenberg-Kohn theorem, which is the theoretical basis of DFT, was proved, and Kohn-Sham method, which is the practical method of DFT, was proposed. In 1970s, DFT was commonly used in solid-state physics. In 1980s, DFT was commonly used in other area of physics and chemistry. In 1990s, the exchange-correlation functionals in DFT were improved, and have been used in quantum chemistry. DFT has an advantage in treating electronic correlations, while it has a shortcoming in treating electronic exchange interactions. Recently, Lee, Yan and Parr functionals for correlation, and Becke's 1988's functionals for exchange are widely used. Hybrid type potentials are used in order to incorporate the exchange interactions in Hartree-Fock theory. Especially, Becke's three parameters potential (B3LYP) is widely used. These parameters are determined by fitting to the well-known systems, and there are no systematic method to improve the precisions of calculation.

Other methods to calculate the quantities in quantum systems with high accuracy are post-Hartree-Fock methods. These include MP (Moeller-Plesset) method, CI (Configuration interaction) and CC (Coupled Cluster) method. In these methods, the linear combination of Slater determinants is used as the wave function of the system.

Basis set

In practical calculations, the molecular orbitals need to be expanded by the well-known basis in both cases of molecular orbital method and Kohn-Sham's DFT. Even for many atomic molecular systems, we can use the basis functions based on the hydrogen type atomic orbitals. We call the basis functions, which are the solutions of Schroedinger equation of hydrogen type atoms, as Slater type orbitals(STO). In molecular orbital method, most CPU time is spent in the calculation of the integration of the products of three quantities: 1) basis function, 2) potentials and 3) complex conjugate of basis. Since STO has the form of $\exp(-\alpha|r|)$, the calculations take much time. On the other hand, since Gaussian type orbitals (GTO) has the form of $\exp(-\alpha r^2)$, the calculations take less time. GTO has the round form around the origin, while STO has the sharp form around the origin. A linear combination of GTO can be fitted to the form of STO. This linear combination of GTO can be regarded as a basis set, and is called contracted GTO (CGTO). On the other hand, the "uncontracted" GTO is called primitive GTO (PGTO). For example, we explain the meaning of 6-31G as the following; the number 6 means we use a CGTO consisting of 6 PGTOs for inner shell. The number 31 means we use a CGTO consisting of 3 PGTOs, and a PGTO for valence

shell. In order to take into account the polarization of electric charge in atoms and molecules, the basis with higher azimuthal quantum number can be added to the basis set. In 6-31G*, which is also denoted by 6-31G(d), six d bases are added to 6-31G for the atoms except hydrogen. In 6-31G**, which is also denoted by 6-31(d, p), three p bases are added to 6-31G* for the hydrogen atoms.

1.1.2 Signal transduction in the cell

Signal acts in various combinations and regulates the behavior of the cell. Most of the signals in the cell is the local mediation substances. Some of them bind the outer surface of the cell and perform the transduction by the contact.

The signal transduction between the cells needs the signal molecule outside the cell and the complementary receptor protein group which exists in the target cell and binds to the specific signal molecule. Most of the signal molecules outside the cell are hydrophilic and cannot pass the cell membrane. These molecules activate the receptor proteins on the surface of the target cell, and the receptor convert the outer signal to the inner signal. The inner signal changes the behavior of the target cell.

There are three ways of the cell surface receptors to convert the outer signal: 1) ionotropic receptor is opened and closed, depending on the binding neurotransmitter, 2) the G protein-coupled receptor (GPCR) indirectly activates and inactivates the membrane bound enzyme and the ion channel through the trimeric GTP-binding proteins. 3) enzyme linked receptor acts as a enzyme or acts with the other enzyme such as protein-kinase which phosphorylate the receptor of the target cell and the specific signal protein.

When the enzyme linked receptor and the GPCR are activated, series of inner signal proteins are activated and mediate the signals. Some of signal proteins convert, amplify or spread the signal, and some of signal proteins integrate the multiple signals from the different paths. Most of these signal proteins act as a temporary activated switch by the phosphorylation and the GTP binding. The target cell regulates the response to the extracellular signal using various mechanisms such as the feedback loop.

After the GPCR stimulates the G protein, the membrane bound enzyme and ion channel are activated or inactivated. The structure of G protein changes and the α subunit and $\beta\gamma$ complex are activated. These regulate directly the activity of the target protein on the membrane. Because the signal transduction mediated by the GPCR is amplified largely by the chain

reaction, the thousands of target proteins are changed even when only one extracellular signal bind to the GPCR. The response mediated by the GPCR stops promptly when the extracellular signal is removed. The α subunit is stimulated by the target protein or by the regulator of G protein signaling, and the α subunit hydrolyzes the bound GTP to GDP leading itself inactivated.

There are various kinds of enzyme linked receptors. In mammalian cell, there are many receptor tyrosine kinase (RTK) and tyrosine kinase associated receptors. When the ligand binds the RTK, the cytoplasmic side area of the receptor phosphorylates multiple tyrosine residues and activates kinase making the multiple phosphorylated tyrosine, which is the junction site of the series of intracellular signal protein through the SH2 domain or PTB. Some juncture proteins act as the adapter of the receptor and Ras-GEF (Sos), which activate the monomeric GTPase Ras. Ras activates three component MAP kinase module, which phosphorylates the gene regulatory protein in the nuclei, transmitting the signal to the nuclei.

1.1.3 Proteins

Most of the dry weight of the cell is made of proteins. Protein is not only the building material of the cell but also is responsible for most of the functions of the cell, such as the catalysis of chemical reaction in the cell and the outward and inward transport of substances across the cell membrane. Proteins are also involved with the signal transduction between the cells and the signal transduction from the cell membrane to nucleus. A small protein, kinesin, moves the organelle in the cell and topoisomerase disentangles a snarled DNA. Protein plays the central role of most of the functions in the cell.

Protein has complicated structure and sophisticated function, from the point of view of chemistry. The functions of proteins are rich in diversity.

The three-dimensional conformation of protein is determined by the amino acid sequence. The noncovalent bond interactions between the areas of polypeptide stabilize the folding structure of the protein. The amino acid with hydrophobic side chain tends to assemble in the inner area of the protein, the structures of $\alpha-$helix and $\beta-$sheet are formed by the local hydrogen bond between the peptide bonds close to each other.

Small protein is usually made from a domain, and large protein is made from the domains connected by the polypeptide chains with various length.

A protein is not a hard lump, but its parts are moving. This mechanical motion is connected with a chemical reaction. This coupling of the chemical reaction and the mechanical motion gives the protein the ability to support the dynamic processes in the cell.

There is a mechanism leading an activity of protein by binding the specific molecule. The capacity of a protein to identify another molecule is important for the functions such as catalysis, signal receptor, switch, motor and small pump.

Protein is regarded as a chemical device. The function of the chemical device depends on the chemical characteristics of the surface of the molecule. At the ligand binding site which exists in the hollow made by the folding of the protein, the amino acid residues are arranged precisely. These residues generate and cleavage the covalent bond in conjunction with each other. Enzyme binds directly the high free energy transition state of the substrate and speeds up the reaction rate. Enzyme can perform acid catalysis and basic catalysis simultaneously. The reaction rate is usually very high and is limited only by the diffusion.

When the ligand binds to the surface of the protein, the protein deforms reversibly. The allosteric conformation change caused by a ligand has the

influence of the binding of another ligand. The relation between these ligands is important for the regulation mechanism of the reactions in the cell. Using the chemical energy, the deformation of the protein can be pushed in one direction.

1.1.4 Cancers

The environmental factor promotes the start and the progress of the tumor. The tumor promoter induces the inflammatory response and makes the local environments such as the change of the gene expression, the stimulation of the cell proliferation and the increase of the mutant cell population generated by the tumor initiator.

The important gene for canceration is classified into two groups, one is the gene in which the acquisition of the function causes the canceration, the other is the gene in which the loss of the function causes the canceration. The canceration is also called the malignant transformation. This is the process by which cells acquire the properties of cancer.

The gain-of-function mutation, which changes the protooncogene to the oncogene, causes improperly the cell proliferation. An oncogene is a gene that has the potential to cause cancer. The loss-of-function mutation of the

antioncogene abolishes the inhibitory function which helps suppressing the number of cell.

The oncogene is generally dominant, while the antioncogene is generally recessive. In tumor cells, they are often mutated or expressed at high levels. Most normal cells undergo a programmed form of death (apoptosis). Activated oncogenes can cause those cells that ought to die to survive and proliferate instead. Anti-oncogene is a gene which protects a cell from one step on the path to cancer. When this gene is mutated to cause a loss or reduction in its function, the cell can progress to cancer, usually in combination with other genetic changes.

The individual, who has both genes of deletion form and of functional form, tends to have tumor, because the tumor cell is generated when either the loss of normal gene or the loss-of-function mutation occurs.

Once the candidate gene is found, we can assess the importance of the candidate for the canceration using the mouse. If it is the candidate of the oncogene, we can use the overexpression. If it is the candidate of the antioncogene, we can use the inactivation.

The study of the embryogenesis and the mutant mouse is useful in the elucidation of the functions of many genes important for the canceration.

Many of oncogene and antioncogene mutated in tumor cell direct the elements constructing the regulation pathway of the growth, division, differentiation and death of the cell.

DNA tumor virus occasionally promotes the canceration by generating the inhibitory protein of the product of the antioncogene.

The stepwise progress of the tumor is often related to the mutation involved with the activation of the specific oncogene and with the inactivation of the specific antioncogene. These relations are most understood in the colon cancer. The combinations of found mutation and epigenetic change are different from each other among not only different kinds of cancers but also different patients of the same disease. This means that these mutations occur randomly. However, the same type of mutation is often seen. In biology, and specifically genetics, epigenetics is the study of heritable changes in gene expression or cellular phenotype caused by mechanisms other than changes in the underlying DNA sequence - hence the name epi- (Greek: $\varepsilon\pi\iota$- over, above, outer) - genetics. It refers to functionally relevant modifications to the genome that do not involve a change in the nucleotide sequence.

The prevention, diagnosis and treatment of the cancer is improved by the recent understanding of the biology of the cancer.

The tumor cell has the following characteristics: 1) the dependence on the oncogene, 2) the loss of DNA repair mechanism, 3) the loss of the cell cycle checkpoint mechanism and 4) the loss of the regulation path of apoptosis. For the development of the drug which thrusts the indispensable molecule to the proliferation and the survival of the cancer cell and kills the cancer cell, it is important to understand the regulatory mechanism in the normal cell and to understand precisely how the mechanism is destroyed by the cancer.

1.2 Hras protein

We investigate Hras protein, which belongs to Ras family. Ras family is a member of small GTPase, which belongs to G-protein. So, I start with the explanation of G-protein. In this section, we use the description in Ref. [27].

1.2.1 G-protein

G-protein is the abbreviation for guanine nucleotide binding protein, and is a family of proteins which are involved with second messenger cascade.

1.2.2 Small GTPase

Small GTPase or small GTP binding protein is one of the family of GTP binding protein with small molecular mass (20-25 kDa). Small GTPase acts as a molecular switch of signal transduction in the cell, which binds guanosine triphosphate (GTP), hydrolyzes GTP to GDP and exchanges GDP for GTP. The representative one is a product of proto-oncogene *ras*. Because each of small GTPase is highly homologous to ras protein, small GTPases is also called Ras superfamily.

Signal transduction

Although small GTPase is also called small G-protein, small GTPase is different from the G-protein in the narrow sense (trimeric G-protein) in many aspects while small GTPase is partially similar to the trimeric G-protein in the structures and the functions. Small GTPase acts as a molecular on/off switch corresponding to the states binding GTP/GDP, which is controlled by the proteins of GDP/GTP exchange factor (GEF) and GTPase-activating protein (GAP). Small GTPase is associated with the regulations of various functions in the cell, such as the multiplication of the cell, the differentiation of the cell, the motion of the cell and the transportation of lipid vesicle.

Subfamily of Ras superfamily

More than one hundred kinds of Ras superfamily have been known. They are specified to five subfamilies, Ras, Rho, Rab, Arf and Ran by phylogeny. Each subfamily has been known to have a specific function.

Ras family: A member of Ras family is located on the signal transduction pathway from the tyrosine kinase receptor, and is involved with the regulation of cell proliferation. While especially Ras and Rap have been investigated, Rheb is investigated recently.

Rho family: A member of Rho family is involved with regulation of the cytoskeleton. Especially RhoA, Racl and Cdc42 have been investigated in detail.

Rab family: A member of Rab family is involved with the vesicular transport.

Arf family: A member of Arf family is involved with the vesicular transport.

(A member of one of the families mentioned above can be lipid-linked (prenylated) and localized at plasma membrane.)

Ran family: A member of Ran family is involved with transport between

the nucleus and cytoplasm.

1.2.3 Ras family

Ras family (Ras protein, Ras subfamily) is a kind of small GTP binding proteins, and a molecule which is involved with many events in the cell, such as transcription, cell growth, acquisition of motility of the cell and inhibition of cell death. Because abnormal Ras is deeply involved with canceration of the cell, *ras* gene is a kind of proto-oncogene.

Because Ras was found in Rat sarcoma, Ras was named after that.

Ras has a mass of about 21 kDa, has a region binding GTP or GDP and has a region, named effector loop, which is for the interaction with PI 3-kinase (PI3K), Raf and Ral-GEF. Ras has a tail of lipid in C-terminal, which is used for anchoring Ras to plasma membrane. Cancerous Ras often has a missense mutation at Gly12 or Gln61, which is located in the part of GTP binding region.

Ras is in the inactivated state when Ras binds to GDP. When this GDP is exchanged to GTP by guanine nucleotide exchange factor (GEF), Ras is activated. It is known that Ras is activated through some molecules by actual all receptor tyrosine kinase (tyrosine kinase receptor) (RTK), including

PDGF (platelet-derived growth factor), NGF (nerve growth factor) and EGF (epidermal growth factor) and so on.

1.2.4 Hras

GTPase Hras, also known as transforming protein p21, is an enzyme encoded by human *HRAS* gene. *Hras* gene is located at 15.5 of short arm in chromosome 11, and is from 522,244 bp to 525,549 bp.

GTPase Hras is associated with the control of cell division in response to the impulse of the growth factor. The growth factor acts by binding the receptor on the surface of the cell extended in somatic membrane. Once activated, the receptor promotes the signal transfer process, by which the protein and the second messenger mediate the signal from outside to nucleus and order cell to grow and divide. Hras protein is a GTPase, is an early player in many signal propagating pathways and binds somatic membrane by existence of the isoprenyl group at C-terminal. Hras acts as a molecular on/off switch: once it turns on, it recruits and activates the proteins needed for propagating the signal from the receptor, for example c-Raf or PI 3-kinase. Hras binds GTP in the activated state, and has ability of intrinsic hydrolysis, in which it dissociates the terminal phosphate of GTP and changes GTP to GDP.

With transferring of GTP to GDP, Hras turns off. The rate of transferring is usually slow, but can be speeded up drastically by the accessory protein of GTPase activating proteins (GAP), for example RasGAP. In turn, Hras can bind the proteins of the guanine nucleotide exchange factors (GEF), which force binding nucleotide to dissociate from Hras, for example SOS1. Subsequently, Hras binds GTP in the cytosol, Hras-GTP is dissociated from GEF, and Hras is activated. Hras belongs to Ras family, which includes two other proto-oncogene Kras and Nras. These proteins are controlled in the same manner, and appear differently in the site of activation.

Costello syndrome

Costello syndrome is a disease whose properties are mental retardation, distinctive facial features and problems in heart. At least five mutations of Hras gene have been identified in patients of Costello syndrome. Each of these mutations changes one amino acid (single protein product element) of the essential region of the Hras protein. The most common mutation substitutes the 12th amino acid glycine by amino acid serine (denoted by Gly12Ser or G12S). The mutations responsible for Costello syndrome lead to the production of sustainable activated Hras proteins. These hyperactivated Hras

proteins order cells to grow and divide permanently, instead of triggering the cell growth in response to the proper signal from the outside of the cell. This uncontrollable cell division can lead to the production of the noncancerous and cancerous tumors. Although researchers are not sure how the mutations of Hras gene bring other properties of Costello syndrome (mental retardation, distinctive facial features and problems in heart), overgrowth of the cell and unusual cell division may cause many symptoms and signs.

Bladder cancer

Hras has been shown to be a proto-oncogene. When mutated, proto-oncogene has potential to change the normal cell to cancerous cell. Some mutations of the gene are acquired in human's life span, and exist only in some cells. These changes are called the somatic mutation, and are not inherited. A somatic mutation of Hras gene in bladder cell is associated with bladder cancer. One typical mutation is often identified in bladder tumor. This mutation substitutes one amino acid of Hras protein to another amino acid. Specifically, the mutation substitutes the 12th amino acid glycine to amino acid valine (denoted by Gly12Val or G12V). Transformed Hras protein is persistently activated in the cell. This hyperactivated protein orders cell to

grow and divide in spite of the absence of the signal from outside, and leads to the uncontrollable cell division and the formation of tumors. The mutations of Hras gene are also associated with the progress of bladder cancer, and increase the risk of tumor recurrence after treatment.

Other cancers

The somatic mutations of Hras gene can be associated with the progress of some other types of cancer. These mutations lead the Hras proteins which are always activated and can order cells to grow uncontrollably and divide. Recent researches suggest that the mutations of Hras are observed in thyroid cancer and kidney cancer.

1.3 Overview of this thesis

In chapter 2, we describe the potentials of the atoms around Mg^{2+} in the Hras GTP and GDP complexes. In chapter 3, we show our calculations of molecular dynamics simulations of the Hras GTP and GDP complexes. Chapter 4 is discussion, and chapter 5 is conclusion of the thesis.

Chapter 2

Potentials of the Atoms around Mg^{2+} in the Hras GTP and GDP Complexes

In this chapter, we study the quantum state around Mg^{2+} ion in the H-ras GTP complex and in the H-ras GDP complex in order to understand the hydrolysis of the GTP to GDP in the H-ras complex, which plays the key role in overcoming human cancer. We calculated the force fields and the atomic charges around Mg^{2+} ion in the H-ras GTP complex and in the H-ras GDP complex in the B3LYP level using a basis functional set 6-31G**.

The calculation was performed in the subsystem consisting of the bases or the molecules which contain the oxygen having a coordinate bond to the Mg^{2+} ion. Our calculation shows that the oxygen atoms in both GTP and GDP bind tightly to the Mg^{2+}, although the oxygen atoms in the H_2O bind loosely. We performed MD simulations of H-ras GTP complex and H-ras GDP complex in solution using these potential parameters. We have shown that the structure differences between the H-ras GTP complex and H-ras GDP were found in the loop 2 and the loop 4 mainly. The loop 2 is the second loop and the fourth loop from the N-terminal of H-ras protein. Here, the loop 2 consists of 26–37 residues and the loop 4 consists of 58–68 residues.

2.1 Introduction

H-ras proteins, the products of the *ras* onco- and protooncogenes, are guanine nucleotide binding proteins, which act as molecular switch. In the active state, H-ras proteins are bound to guanosine triphosphate (GTP), and in order to switch to the inactive state, the γ-phosphate of the nucleotide has to be hydrolyzed. In the oncogenic mutation, this reaction is suppressed. Understanding this reaction is very important to overcome human cancer,

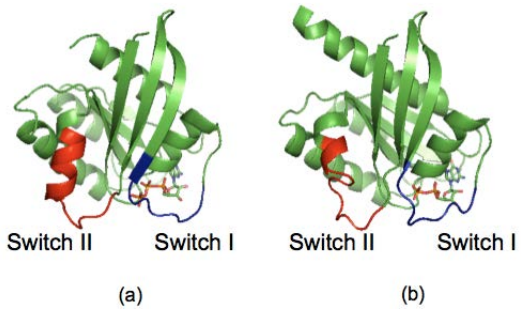

Figure 2.1: The structure of the switch regions in the H-ras GTP complex (a) and in the H-ras GDP complex (b). The figures are drawn using the PDBID:121P (a) and PDBID:1Q21 (b). In (a), we substituted GTP in place of GCP in PDBID:121P.

because H-ras proteins frequently mutate to be activated in a variety of human cancer cells [28].

The structures of active H-ras GTP complex [29] and inactive H-ras GDP complex [30] have been investigated by x-ray crystallographical analyses. These analyses revealed that there are structural changes in so called switch I and II regions, which are around the nucleotide binding site, between the two complexes. Fig. 2.1 shows the switch regions in the H-ras GTP complex (a) and in the H-ras GDP complex (b). Switch I consists of 30-38 residues, which form loop 2 and a part of $\beta 2$ strand. Switch II consists of 60-72 residues, which form loop 4 and $\alpha 2$ helix (The names of loops, loop 2 and loop 4, are shown later in Fig. 2.7.) It is known that the structural changes

described above arise from the differences of the following (a) and (b): (a) the coordination bond of Thr35 and the hydrogen bond of Gly60 in the H-ras GTP complex, (b) the coordination bond of Thr35 and the hydrogen bond of Gly60 in the H-ras GDP complex. [31–37]. It is also known that Thr35 and Gly60 are conserved in Ras family, and the mutation of these amino acids makes the hydrolysis of GTP slower [31–37].

In order to understand this hydrolysis, we have to know the structures of the H-ras GTP complex and the H-ras GDP complex with the solvent. We can sample these structures by molecular dynamics simulations. Parameter sets which are widely used for typical biological molecules are given in AMBER force field [38]. When we perform the molecular dynamics simulation of the protein containing metal atoms or ions, we need the parameter set of the potential describing the displacement of the atoms around the metal particle. However, the parameter set of the H-ras GTP complex and the H-ras GDP complex containing Mg^{2+} are not included in AMBER.

In the following, we mention the works of five papers on the calculations of the parameters of the H-ras GTP complex and the H-ras GDP complex. (1) Foley *et al.* performed MD simulations of the H-ras GTP complex [39]. In order to perform MD simulations, they calculated the force field and the atomic

charges using 3-21G* basis set. They rescaled the atomic charges to the 6-31G** basis set. However, the parameter was not included in their papers, and the treatment of the coordination bond between an oxygen and Mg^{2+} was not discussed in their papers. They used GAUSSIAN88 [40] for *ab initio* quantum mechanics calculations. *Ab initio* molecular orbital method they used is not mentioned in the paper. (2) Worth *et al.* calculated the atomic charges in the H-ras GTP complex and in the H-ras GDP complex [41]. They used the 3-21G* basis set and, only for the phosphorus. They added the sp-orbital wave function from 6-31G* basis set. They used GAUSSIAN88 [40] for *ab initio* quantum mechanics calculations. *Ab initio* molecular orbital method they used is not mentioned in the paper. It is not clear whether the basis set is consistent with the present AMBER force fields and the atomic charges. They did not treat directly the coordination bond between an oxygen and Mg^{2+}. (3) Mello *et al.* performed the MD simulations of the H-ras GTP complex [42]. They used the parameter set for the proteins in the water of GROMOS. GROMOS is a force field for molecular dynamics simulation developed at the University of Gromingen and at Computer-Aided Chemistry Group at the Laboratory for Physical Chemistry at the ETH Zurich. The parameters of GROMOS are different from the parameters of AMBER.

In that paper, they did not write directly the force field and the atomic charges around Mg^{2+}. (4) Futatsugi *et al.* performed the MD simulations of the H-ras GTP complex [43]. They calculated the force field and the atomic charges around Mg^{2+} using 6-31G** basis set at the Hartree-Fock level. However, their parameters were not written in their paper. The treatment of the coordination bond between an oxygen and Mg^{2+} was not discussed in their papers. (5) Kobayashi *et al.* performed the MD simulations of the H-ras GTP complex and the H-ras GDP complex [44]. They used the parameters for guanine nucleotides determined by Meagher *et al.* [45], in which the parameters of the GTP-protein complex and of the GDP-protein complex were not calculated directly. The force fields and the charges around Mg^{2+} were not discussed in their papers.

In this chapter, we created the force field and charges for GTP and Mg^{2+} in the H-ras GTP complex and for GDP and Mg^{2+} in the H-ras GDP complex using Gaussian09 [46]. Calculations were performed in the B3LYP level, using a basis set, 6-31G**. Namely, we calculated the force field and atomic charges around Mg^{2+} explicitly with a large basis. We define the Mg-subsystem as a system which consists of both Mg^{2+} and such molecules and amino acid residue that contain oxygen having a coordination bond to

Mg^{2+}. We calculated quantum chemically the energy of the Mg-subsystem with various positions of the oxygen binding coordinately to Mg^{2+}, so that we obtain the parameter set of the potential of this system with respect to the displacement of the oxygen binding coordinately to Mg^{2+}. At the same time, we calculated the molecular orbitals and the atomic charges in the Mg-subsystem, so that we can use these in the molecular dynamics simulations.

Using calculated potential parameters, we performed the simulations of the H-ras GTP complex and the H-ras GDP complex. In order to check the validity of these potential parameters, we compare the results of these simulations with the results of Kobayashi *et al* [44]. They used the H-ras GNP (phosphoaminophosphonic acid-guanylate ester) complex structure (PDBID:5P21) as their initial structure of their calculation of H-ras GTP complex. In their paper, they call H-ras GTP complex as GTP_2 bound state. They performed MD simulations of GTP_2 bound state and GDP bound state for 50 ns. We compare our results with their results.

2.2 Methods

2.2.1 H-ras GTP complex

Definition of the Mg-subsystem of the H-ras GTP complex and optimization of the position of H atoms

First, we use the H-ras GCP complex structure (PDBID:121P) in the Protein Database (PDB) as our initial structure of our calculation, where GCP (phosphomethylphosphonic acid guanylate ester) is the compound in which the oxygen atom of γ-phosphate in the GTP is replaced by the carbon atom. This replacement is performed in order to reduce the rate of hydrolysis of γ-phosphate in the H-ras GCP complex. For this purpose, besides the H-ras GCP complex, the guanosine 5′-(β,γ-imido) triphosphate (GppNHp) H-ras complex and the 5′-3-*O*-(thio)triphosphate (GTPγS) H-ras complex are used. In this chapter, we used the structure of the H-ras GCP complex as in the paper of Futatsugi *et al* [43]. Next, in our model structure, we replaced the carbon atom in the GCP by the oxygen in order to calculate the potential of the H-ras GTP complex. We added the hydrogen atoms binding to the appropriate atoms in the complex, because the PDB file does not contain the position of the hydrogen atoms. From the definition of the Mg-subsystem

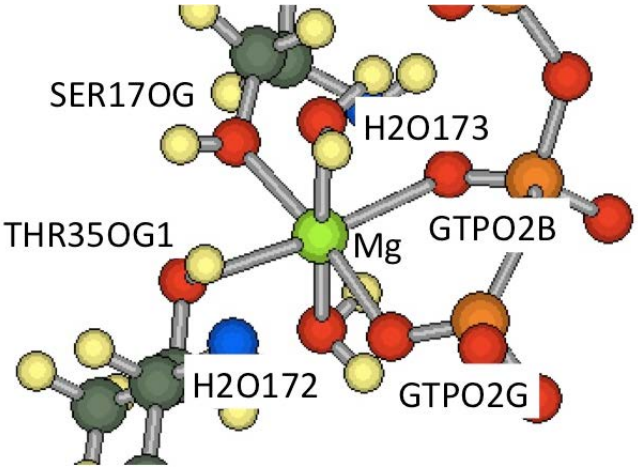

Figure 2.2: The structure of the Mg-subsystem of the H-ras GTP complex

described in the introduction, the Mg-subsystem of the H-ras GTP complex consists of Mg^{2+}, GTP, H_2O172, H_2O173, SER17 and THR35. We focus on Mg^{2+}, because Mg^{2+} is thought to play a key role in GTP hydrolysis in H-ras GTP complex.

In Fig. 2.2, the structure of the Mg-subsystem of the H-ras GTP complex is shown. We optimized the position of the hydrogen atoms so that the position gives the minimum energy of the Mg-subsystem. In this process, we use the Merz-Kollman charges [47] as the atomic charges in order to treat the polarization of atoms in the Mg-subsystem efficiently.

The BOND terms and the ANGLE terms of the potential

We obtain the lengths and the angles which give the energy minimum. We also obtain the quadratic coefficients of the energy with respect to the length and the angles. The AMBER force field is basically determined by the following potential,

$$\begin{aligned} V(r) &= \sum_{\text{bonds}} K_b(b-b_0)^2 + \sum_{\text{angles}} K_\theta(\theta-\theta_0)^2 + \sum_{\text{dihedrals}} (V_n/2)[1+\cos(n\phi-\delta)] \\ &\quad + \sum_{\text{nonb}ij} (A_{ij}/r_{ij}^{12}) - (B_{ij}/r_{ij}^{6}) + (q_i q_j/r_{ij}), \end{aligned} \tag{2.1}$$

where b is the bond length, and K_b is the quadratic coefficient of the bond length b. θ is the bond angle, and K_θ is the quadratic coefficient of the bond angle θ. ϕ and δ are the dihedral angles, and V_n is the coefficient. r_{ij} is the length between i-th and j-th nonbonded atoms, A_{ij} and B_{ij} are coefficients of the attractive and the repulsive parts of Lennard-Jones interaction between i-th and j-th nonbonded atoms, and q_i is the atomic charge of the i-th atom.

We call the first term as the BOND term and the second term as the ANGLE term. We obtain the lengths b_0s, the angles θ_0s, the coefficients K_bs and K_θs from the calculations below.

The BOND terms of the potential are calculated. We select a single oxygen atom which binds coordinately to Mg^{2+}. In order to change the length of the Mg^{2+}-oxygen bond, we move the position of the selected oxygen atom in the direction of the Mg^{2+}-oxygen bond. We calculated the energy of the Mg-subsystem of H-ras GTP complex. We obtain the optimized length which gives the minimum energy of the Mg-subsystem, and obtain the quadratic coefficients of the Mg-subsystem energy with respect to the Mg^{2+}-oxygen bond length.

The ANGLE terms of the potential are calculated. We select two oxygen atoms which bind coordinately to Mg^{2+}. One of the two selected atoms is moved on the plane which contains Mg^{2+} and two selected oxygen atoms, in order to change the angle O-Mg^{2+}-O. We calculated the energy of the Mg-subsystem of H-ras GTP complex. At the same time, other angles change, so we use some relations together in order to derive the optimized angle which gives the minimum energy of the Mg-subsystem, and we derive the quadratic coefficients of the Mg-subsystem energy with respect to the angle O-Mg^{2+}-O.

Comments on other potentials are followings. In general, we should obtain the optimized torsion angles and the quadratic coefficients of energy with respect to dihedral angles. In this chapter, we assume that we can neglect the dihedral term of the potential energy in the Mg-subsystem.

We mention the following for nonbonding terms. We assume that, even in the H-ras complexes, we can use the values of L-J parameters of the Mg^{2+} in water. For Coulomb terms, we use atom-centered charges calculated in the subsystem.

2.2.2 H-ras GDP complex

For the H-ras GDP complex, we did the same procedure as for the H-ras GTP complex except for the following part.

We use the H-ras GDP complex structure (PDBID:1Q21) in the Protein Database (PDB) as our initial structure of our calculation, where no substitute compound is used because GDP is stable in the H-ras GDP complex.

From the definition of the *Mg-subsystem* described in the introduction, the Mg-subsystem of the H-ras GDP complex consists of Mg^{2+}, GDP, H_2O201, H_2O202, H_2O203, H_2O204, and SER17. In Fig. 2.3, the structure of the Mg-subsystem of the H-ras GDP complex is shown.

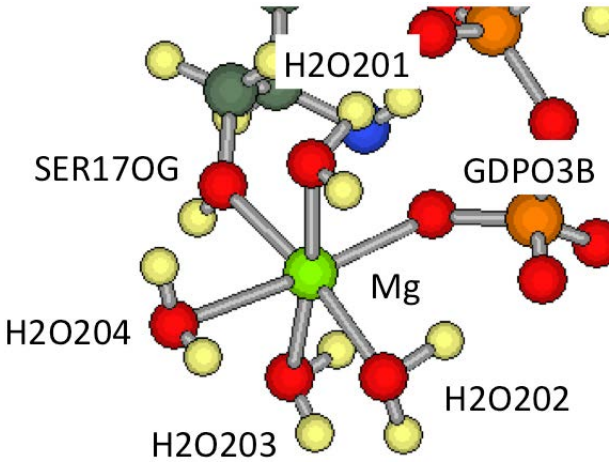

Figure 2.3: The structure of the *Mg-subsystem* of the H-ras GDP complex

2.2.3 MD simulations

We performed MD simulations for the H-ras GTP complex and for the H-ras GDP complex. The initial structures were obtained from the x-ray structures (PDBID:121P) for the H-ras GTP complex and (PDBID:1Q21) for the H-ras GDP complex.

All MD simulations were performed with the AMBER11 program [48]. Amber ff03 [38] with our modified potential parameters described above around Mg ion was used for the proteins and ions, and TIP3P [49] was used for water molecules. We modified the parameters for guanine nucleotides originally determined by Meagher *et al* [45]. We used our modified parameters described above. The number of water molecules was 22,265 for H-ras

GTP complex and 21,740 for H-ras GDP complex. Ten Na^+ counterions were added for charge neutralization in the case of the H-ras GTP complex, and six Na^+ were added in the case of H-ras GDP complex. The particle mesh Ewald method with cubic interpolation was applied to the long-range electrostatic interactions. The cut-off length of the short-range Coulomb and the van der Waals interactions was 12 Å. Bonds involving hydrogen atoms were constrained with the SHAKE algorithm. The water position was optimized, while the atoms of the complex of protein and guanine nucleotide were restrained by harmonic potential. The temperature of the water was heated up from 100K to 300K with a Langevin thermostat. Then the restraints of the atoms of the complex of protein and guanine nucleotide were weakened gradually under the NPT conditions at 300K. After the initial equilibration period, an additional simulation was carried out under the NPT conditions at 300K with a Langevin thermostat for about 1 ns. We used the pressure coupling algorithms of weak-coupling variety, provided in Amber, analogous to temperature coupling [50]. Pressure relaxation time was 1 ps.

2.3 Results

In this section, we show the results of quantum calculation of Mg-subsystem in 2.3.1 and the results of MD simulations of the H-ras GTP complex in water and the H-ras GDP complex in water in 2.3.2.

2.3.1 Differences in Mg-subsystem between H-ras GTP complex and H-ras GDP complex

In this subsection, we show the results of quantum calculation of Mg-subsystem. We show the total charge, the atomic charges, and the parameters in the BOND term and in the ANGLE term. We also show the molecular orbitals in the followings.

The total charge of Mg-subsystem

When we calculate the energy of the Mg-subsystem of H-ras GTP complex quantum chemically, we put the charge of the Mg-subsystem as -2, because the charge of Mg^{2+} is $+2$, the charge of GTP is -4, the charge of H2O is 0, and the charge of amino acid residue is also 0. In Fig. 2.4 (a), the chemical structure of GTP is shown.

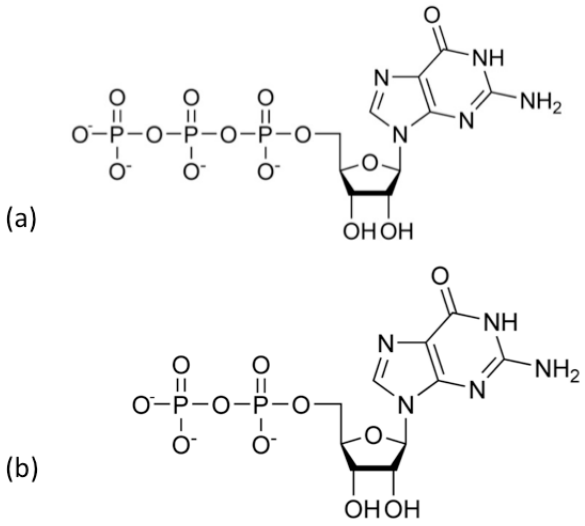

Figure 2.4: The chemical structure of GTP (a) and GDP (b)

On the other hand, when we calculate the energy of the Mg-subsystem of H-ras GDP complex quantum chemically, we put the charge of the Mg-subsystem as -1, because the charge of Mg^{2+} is $+2$, the charge of GDP is -3, the charge of H2O is 0, and the charge of amino acid residue is also 0. In Fig. 2.4 (b), the chemical structure of GDP is shown.

The atomic charges of the Mg-subsystem

In Table 2.1-2.4, our results of the atomic charges of the Mg-subsystem in the H-ras GTP complex and the H-ras GDP complex are shown.

From Table 2.1, the difference between the H-ras GTP complex and the

atom	GTP	GDP	atom	GTP	GDP
O3G	-0.746		H3'	0.115	0.063
O2G	-0.698		C2'	-0.004	-0.061
O1G	-0.689		O2'	-0.604	-0.620
PG	0.942		HO'2	0.385	0.427
O3B	-0.465	-1.108	H2'1	0.153	0.112
O2B	-0.755	-0.737	C1'	0.443	0.417
O1B	-0.650	-0.724	H1'	-0.021	0.079
PB	0.929	1.053	N9	-0.204	-0.176
O3A	-0.353	-0.362	C8	0.252	0.251
O2A	-0.684	-0.592	H8	0.140	0.110
O1A	-0.614	-0.724	N7	-0.529	-0.527
PA	0.921	0.849	C5	0.105	0.069
O5'	-0.433	-0.176	C6	0.481	0.558
C5'	0.015	-0.264	O6	-0.540	-0.559
H5'1	0.131	0.165	N1	-0.482	-0.675
H5'2	0.083	0.131	H1	0.322	0.385
C4'	-0.017	0.320	C2	0.570	0.773
H4'	0.071	0.062	N2	-0.757	-0.851
O4'	-0.376	-0.482	H21	0.327	0.364
C3'	0.252	0.152	H22	0.352	0.377
O3'	-0.653	-0.626	N3	-0.577	-0.664
H3T	0.404	0.415	C4	0.291	0.228

Table 2.1: The atomic charges of the Mg-subsystem (GTP and GDP) of the H-ras GTP complex and the H-ras GDP complex.

atom	H-ras GTP	H-ras GDP
Mg	1.037	1.297
SER17:N	-0.812	-0.556
SER17:H	0.562	0.347
SER17:CA	-0.425	-0.318
SER17:HA	0.170	0.180
SER17:CB	0.306	0.192
SER17:HB2	-0.030	0.078
SER17:HB3	0.032	0.055
SER17:OG	-0.478	-0.658
SER17:HG	0.370	0.437
SER17:C	0.687	0.656
SER17:O	-0.612	-0.576

Table 2.2: The atomic charges of the Mg-subsystem (Mg and SER17) of the H-ras GTP complex and the H-ras GDP complex.

atom	charge	atom	charge
H2O172:HW1	0.398	THR35:CB	0.201
H2O172:HW2	0.526	THR35:HB	0.098
H2O172:OW	-0.881	THR35:CG2	-0.355
H2O173:HW1	0.444	THR35:HG21	0.089
H2O173:HW2	0.411	THR35:HG22	0.131
H2O173:OW	-0.795	THR35:HG23	0.076
THR35:N	-0.742	THR35:OG1	-0.581
THR35:H	0.371	THR35:HG1	0.302
THR35:CA	0.589	THR35:C	0.272
THR35:HA	-0.052	THR35:O	-0.442

Table 2.3: The atomic charges of the Mg-subsystem (H2O and THR35 in H-ras GTP) of the H-ras GTP complex and the H-ras GDP complex.

atom	atomic charge
H2O201:HW1	0.439
H2O201:HW2	0.545
H2O201:OW	-0.926
H2O202:HW1	0.398
H2O202:HW2	0.407
H2O202:OW	-0.796
H2O203:HW1	0.406
H2O203:HW2	0.414
H2O203:OW	-0.815
H2O204:HW1	0.398
H2O204:HW2	0.408
H2O204:OW	-0.737

Table 2.4: The atomic charges of the Mg-subsystem (H2O in H-ras GDP) of the H-ras GTP complex and the H-ras GDP complex.

H-ras GDP complex is large for O3B. In H-ras GTP complex, this atom belongs to inner phosphate group and does not bind to Mg^{2+} coordinately. In H-ras GDP complex, this atom belongs to the outer phosphate group and binds to Mg^{2+} coordinately.

From Table 2.2, the atomic charge of Mg^{2+} in the H-ras GTP complex is not +2 but +1.037 and the atomic charge of Mg^{2+} in the H-ras GDP complex the atomic charge of Mg^{2+} is not +2 but +1.297, by the influence of the coordinate bonds by six oxygen atoms.

From Table 2.3 and 2.4, we can find that OW of H2O172 in H-ras GTP complex and OW of H2O1 in H-ras GDP have larger negative charges than

that of TIP3P model (-0.834), although OWs of other H2O molecules have almost the same negative charge as TIP3P model. Those are caused by the anisotropy of the electric fields around Mg^{2+} in direction, since distances of OWs in H2Os to Mg^{2+} are almost the same.

The differences between our calculated value and the value calculated by Worth *et al.* [41] in H-ras GTP complex are large for PA, O1G and PB. To represent the electronic orbitals with large angular momentum, the following two points are important: (1) the number of the basis set, (2) the number of polarized functions of the basis set. In our systems, the electronic orbitals in P atoms are orbitals with large angular momentum. For two atoms of P (PA and PB), those two points mentioned above cause a large difference between our calculated value and the value calculated by Worth *et al.* [41].

The differences between our calculated value and the value calculated by Worth *et al.* [41] in the H-ras GDP complex are large at PB, O3A and PA. Those differences are also caused by the reasons mentioned in the case of the H-ras GTP complex.

(a) H-ras GTP complex

bond	b_0 [Å]	K_b [kcal mol^{-1} Å^{-2}]
Mg-GTPO2G	1.902	317.28
Mg-GTPO2B	2.077	268.46
Mg-SER17OG	2.276	197.20
Mg-THR35OG1	2.167	152.75
Mg-H2O173	2.106	67.51
Mg-H2O172	2.193	48.21

(b) H-ras GDP complex

bond name	b_0 [Å]	K_b [kcal mol^{-1} Å^{-2}]
Mg-GDPO3B	2.067	210.72
Mg-SER17OG	2.343	173.34
Mg-H2O201	2.116	70.99
Mg-H2O203	2.136	68.98
Mg-H2O202	2.125	60.33
Mg-H2O204	2.165	44.70

Table 2.5: The bond lengths b_0 and the quadratic coefficients K_b in eq. (1) around Mg^{2+} ion in the H-ras GTP complex (a) and in the H-ras GDP comlex (b).

The parameters in the BOND term and in the ANGLE term

In Table 2.5, our results of the bond lengths which give the minimum energy of the Mg-subsystem and the quadratic coefficients K_{b} of the energy of the Mg-subsystem in the H-ras GTP (a) and in the H-ras GDP (b) with respect to the bond length are shown. From the values of the quadratic coefficients K_{b} in the H-ras GTP complex, it is shown that the oxygen atoms in the GTP bind tightly (317.28 and 268.46 kcal mol^{-1} Å^{-2}) to the Mg^{2+} although the O-Mg-O bond in the H_2O bind loosely (67.51 and 48.21 kcal mol^{-1} Å^{-2}). From the values of the quadratic coefficients K_{b} in the H-ras GDP complex, as in the case of the Mg-subsystem of H-ras GTP complex, it is shown that the oxygen atoms in the GDP or in the SER17 bind tightly to the Mg^{2+}, although the ones in the H_2O bind loosely.

Comparing the values in Table 2.5 (a) and the values in Table 2.5 (b), we find the following three points. (1) K_{b} value of Mg-GTPO2B in the H-ras GTP complex and K_{b} value of Mg-GTPO3B in the H-ras GDP complex are almost the same. This means that the strength of binding of GTPO2B to Mg^{2+} in the H-ras GTP complex is almost the same as the the strength of binding of GTPO3B to Mg^{2+} in the H-ras GDP complex. (2) K_{b} value of Mg-SER17OG in the H-ras GTP complex and K_{b} value of Mg-SER17OG in

the H-ras GDP complex are almost the same. This means that the strength of binding of SER17OG to Mg^{2+} in the H-ras GTP complex is almost the same as the the strength of binding of SER17OG to Mg^{2+} in the H-ras GDP complex. (3) $K_{\rm b}$ values of Mg-H2Os in the H-ras GTP complex and $K_{\rm b}$ values of Mg-H2Os in the H-ras GDP complex are almost the same. This means that the strength of bindings of H2Os to Mg^{2+} in the H-ras GTP complex is almost the same as the the strength of bindings of H2Os to Mg^{2+} in the H-ras GDP complex. These three results imply that the corresponding structure of the H-ras GTP complex is as stable as the corresponding structure of the H-ras GDP complex.

In Table 2.6, our results of the bond angles which give the minimum energy of the Mg-subsystem and the quadratic coefficients of the energy of the Mg-subsystem with respect to the bond angle are shown. Here, the results of the H-ras GTP complex are shown in Table 2.6 (a), and the results of the H-ras GDP complex are shown in Table 2.6 (b).

From the value of the quadratic coefficients K_θ in Table 2.6 (a), it is shown that the angle O-Mg-O, in the plane which contain the GTP oxygens and the amino acid oxygens, items 1) - 6) in Table 2.6 (a), are stiff, although the ones which contains the H_2O oxygens, items 7) - 15) in Table 2.6 (a), are

(a) H-ras GTP complex

	bond angle name	θ_0 [°]	K_θ [kcal/mol]
1)	THR35OG1-Mg-GTPO2B	171.17	799.22
2)	GTPO2G-Mg-GTPO2B	98.70	611.15
3)	SER17OG-Mg-GTPO2B	88.36	596.97
4)	GTPO2G-Mg-THR35OG1	89.97	340.10
5)	THR35OG1-Mg-SER17OG	82.71	325.85
6)	GTPO2G-Mg-SER17OG	169.87	142.89
7)	THR35OG1-Mg-H2O172	90.30	128.12
8)	H2O172-Mg-GTPO2B	88.86	128.12
9)	H2O172-Mg-SER17OG	86.95	60.10
10)	GTPO2G-Mg-H2O172	100.52	60.10
11)	H2O173-Mg-H2O172	170.89	54.05
12)	H2O173-Mg-THR35OG1	96.32	49.76
13)	H2O173-Mg-GTPO2B	83.71	49.76
14)	H2O173-Mg-SER17OG	92.22	10.59
15)	GTPO2G-Mg-H2O173	80.90	10.58

(b) H-ras GDP complex

	bond angle name	θ_0 [°]	K_θ [kcal/mol]
16)	GDPO3B-Mg-SER17OG	92.26	689.84
17)	H2O201-Mg-SER17OG	91.58	624.89
18)	H2O202-Mg-SER17OG	80.33	624.89
19)	GDPO3B-Mg-H2O203	89.90	321.52
20)	H2O203-Mg-SER17OG	174.05	168.22
21)	GDPO3B-Mg-H2O201	86.06	143.10
22)	GDPO3B-Mg-H2O202	97.60	143.10
23)	GDPO3B-Mg-H2O204	171.49	54.62
24)	H2O201-Mg-H2O203	91.03	52.27
25)	H2O202-Mg-H2O203	96.52	52.27
26)	H2O201-Mg-H2O204	89.79	17.53
27)	H2O202-Mg-H2O204	87.79	17.53
28)	H2O201-Mg-H2O202	171.98	0.00
29)	H2O203-Mg-H2O204	82.76	0.00
30)	SER17OG-Mg-H2O204	96.86	0.00

Table 2.6: The bond angles and the angle parameters around Mg^{2+} ion in the H-ras GTP complex (a) and in the H-ras GDP complex (b)

flexible. From the value of the quadratic coefficients in Table 2.6 (b), it is shown that the angle O-Mg-O, which contains the GDP oxygen or the amino acid oxygen, items 16) - 23) in Table 2.6 (b), are stiff, although the one which contains only the H_2O oxygens, items 24) - 29) in Table 2.6 (b), are flexible. The angle of the case of 30) SER17OG-Mg-H2O204 is an exception.

Comparing the values in Table 2.6 (a) and the values in Table 2.6 (b), K_θ values of H2O172-Mg-SER17OG and H2O173-Mg-SER17OG and in the H-ras GTP complex have smaller value than K_θ values of H2O201-Mg-SER17OG, H2O202-Mg-SER17OG and H2O203-Mg-SER17OG in the H-ras GDP complex. This means that the angles H2O172-Mg-SER17OG and H2O173-Mg-SER17OG in the H-ras GTP complex are more flexible than the angles H2O201-Mg-SER17OG, H2O202-Mg-SER17OG and H2O203-Mg-SER17OG in the H-ras GDP complex. This implies that the positions of H2Os binding to SER17OG in the H-ras GDP complex is more stable than the positions of H2Os binding to SER17OG in the H-ras GTP complex.

2.3.2 Molecular orbitals in the Mg-subsystem

In Fig. 2.5 (a, b), molecular orbitals in the Mg-subsystem of the H-ras GTP complex are shown. HOMO is shown in (a), and LUMO is shown in (b).

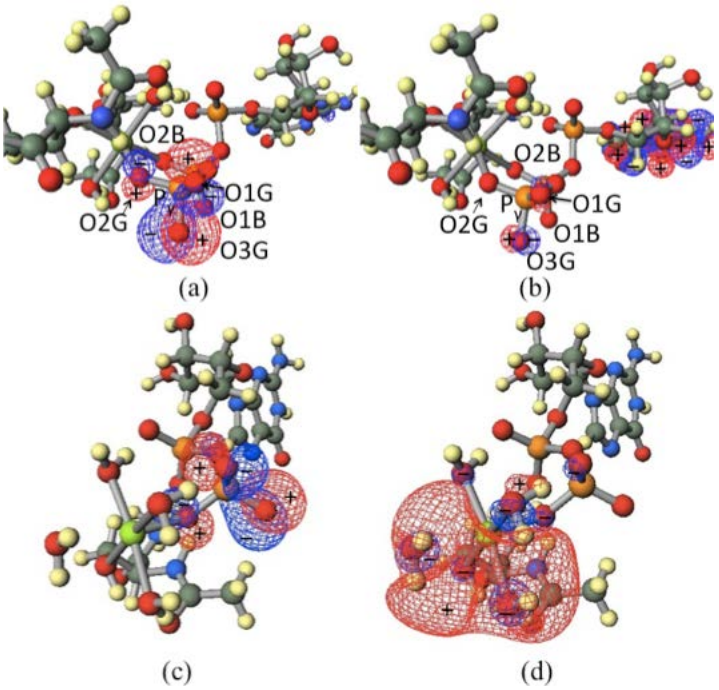

Figure 2.5: Molecular orbitals in the Mg-subsystem of the H-ras GTP complex and H-ras GDP complex. HOMO of the H-ras GTP complex is shown in (a) and LUMO is shown in (b). The positions of atoms are the same in (a) and (b). HOMO of the H-ras GDP complex is shown in (c) and LUMO is shown in (d). The positions of atoms are the same in (c) and (d).

From Fig. 2.5 (a) and (b), it is seen that HOMO spreads widely at O1, O2 and O3 of γ phosphate of GTP, although LUMO shrinks at O1 and O3 of γ phosphate of GTP. In the H-ras GTP complex, because the electronic density of HOMO is high at O1, O2 and O3 of γ phosphate of GTP, it is suggested that electrophiles attack the area of O1, O2 and O3 of γ phosphate of GTP.

In Fig. 2.5 (c, d), molecular orbitals in the Mg-subsystem of the H-ras

GDP complex are shown. HOMO is shown in (c), and LUMO is shown in (d). From Fig. 2.5 (c, d), it is seen that HOMO is dominant around O1, O2 and O3 of β phosphate of GDP, although LUMO is dominant in the area between H2O202, H2O203 and H2O204. In the H-ras GDP complex, because the electronic density of HOMO is high at O1, O2 and O3 of β phosphate of GDP, it is suggested that electrophiles attack the area of O1, O2 and O3 of β phosphate of GDP. And in the H-ras GDP complex, because the electronic density of LUMO is high in the area between H2O202, H2O203 and H2O204, it is suggested that nucleophiles attack the area between H2O202, H2O203 and H2O204.

By comparing Fig. 2.5 (a, b) and Fig. 2.5 (c, d), we can suggest that HOMO is dominant around the oxygens, which belong to the most outside phosphate, which is the γ-phosphate in the case of the H-ras GTP complex and is the β-phosphate in the case of the H-ras GDP complex. This suggests that the most outside phosphate of GTP or GDP has nucleophilic property.

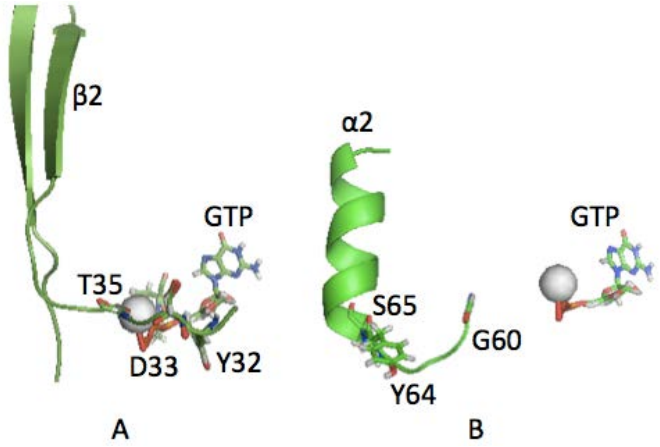

(a) H-ras GTP

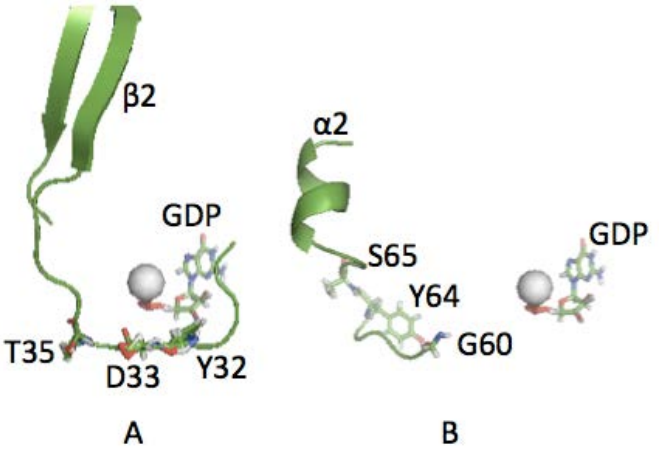

(b) H-ras GDP

Figure 2.6: The structure of switches I (A) and II (B) in the H-ras GTP complex (a) and in the H-ras GDP complex (b)

2.3.3 Differences in conformation between H-ras GTP complex and H-ras GDP complex

We have performed MD simulations of H-ras GTP and H-ras GDP complex using our potentials obtained above. Our results of the structures of switches I and II in the H-ras GTP complex are shown in Fig. 2.6 (a). In Kobayashi *et al.* [44], they obtained the following about the H-ras GTP complex.

- The hydrogen bond between GLY60 and the γ-phosphate makes loop 4 into helical form.
- The first turn of the $\alpha 2$ helix is distorted caused by the helical form of loop 4.

We checked the hydrogen bond between GLY60 and the γ-phosphate. We can find in Fig. 2.6 (a) and Fig. 2.7 that the first turn of the $\alpha 2$ helix is distorted caused by the helical form of loop 4.

Fig. 2.6 (b) shows the structures of switches I and II in the H-ras GDP complex. In Kobayashi *et al.* [44], they obtained the following about the H-ras GDP complex.

- There is a turn in loop 2 in the H-ras GDP complex.

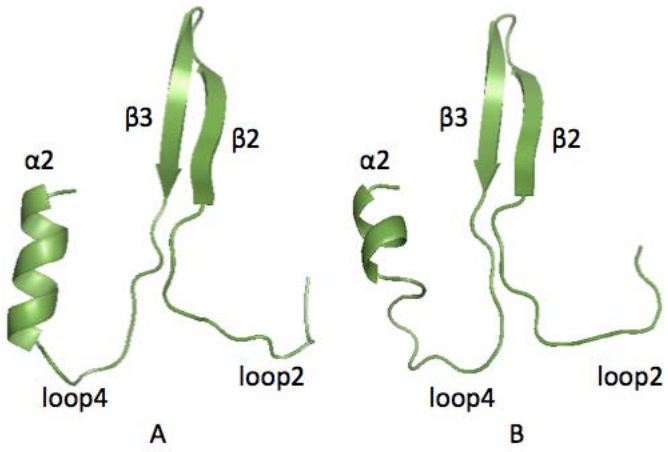

Figure 2.7: The structure of the H-ras GTP complex and H-ras GDP complex

- The first turn of the $\alpha 2$ helix is stable.

In our results, these differences are found in the loop 2, loop 4 and $\alpha 2$ helix (Fig. 2.7).

In Kobayashi *et al.* [44], they obtained the different conformations for loop 2 and loop 4 with different dihedral angles of backbone residues. Fig. 2.8 shows averaged value of the dihedral angles ϕ, involving the backbone atoms C′–N–C$^{\alpha}$–C′, and ψ, involving the backbone atoms N–C$^{\alpha}$–C′–N, of H-ras GTP complex and those of H-ras GDP complex in the switch I and II regions. In Fig. 2.8, we can find the differences between the dihedral angles of H-ras GTP complex and those of H-ras GDP complex in the switch I and II regions.

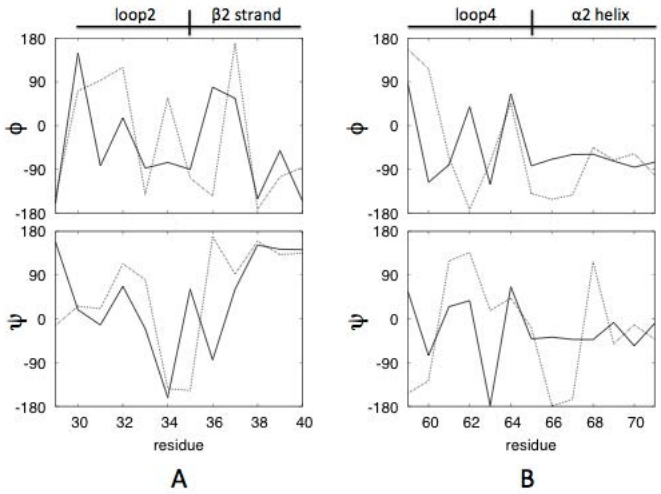

Figure 2.8: Averaged value of backbone ϕ and ψ dihedral angles of residues in switch I(A) and switch II (B). Solid line denotes the values of the H-ras GTP complex, dotted line denotes the values of the H-ras GDP complex.

We compare the results of Kobayashi *et al.* [44] and our results of dihedral angles. The main differences between the results of Kobayashi *et al.* and our results are the following two points. (1) The conformation differences between H-ras GTP and H-ras GDP are observed in slightly different regions in both loop 2 and loop 4. (2) In those regions, each residue has a different form. In Table 2.7, we summarize those differences by specifying the residue number which corresponds to each case.

In the paper of Kobayashi *et al.*, the differences of conformation in loop 2 between H-ras GTP and H-ras GDP were presented as the differences of

the dihedral angles of backbone of PRO34-ILE36 residues. In the H-ras GTP complex, residues PRO34 and THR35 had the extended form ($\psi \sim$ 180), and ILE36 had a wound form (-120 $< \psi <$ 0) . In the H-ras GDP complex, residues PRO34 and THR35 had the wound form, and ILE36 had an extended form.

In our results, the differences of conformation in loop 2 between H-ras GTP and H-ras GDP are presented as the differences of the dihedral angles of backbone of VAL29-ILE36 residues. In the H-ras GTP complex, residues VAL29 and PRO34 have the extended form, GLU31 and THR35 have the wound form, ASP30 and TYR32 have the intermediate form ($-150 < \psi < -120, 0 < \psi < 90$). The dihedral angles of ASP33 and ILE36 are not determined: in a moment they have an extended form, and in another moment they have a wound form. In the H-ras GDP complex, residues TYR32, ASP33 and ILE36 have the extended form, the VAL29 residue has an wound form, the GLU31 residue has an intermediate form, and the dihedral angles of residues ASP30, PRO34 and THR35 are not determined. The dihedral angle of THR35 residue is not determined because the coordination bond between Mg^{2+} and THR35 is missing in H-ras GDP complex.

	Kobayashi	Our results
differences in loop 2	34-36	29-36
GTP extended	34, 35	29, 34
GTP wound	36	31, 35
GTP intermediate		30, 32
GTP not determined		33, 36
GDP extended	36	32, 33, 36
GDP wound	34, 35	29
GDP intermediate		31
GDP not determined		30, 34, 35
differences in loop 4	59-65	59,61-63,66-68
GTP extended	59, 61	63
GTP wound	60, 62-65	62, 66-68
GTP intermediate		
GTP not determined		59, 61
GDP extended	63-65	59, 61, 62, 66, 67
GDP wound		
GDP intermediate		63, 68
GDP not determined	59-62	

Table 2.7: Differences in dihedral angles between the results of Kobayashi *et al.* and our results. The numbers 34, 35, for example, show residue number. The term "differences in loop 2" denotes the resudue regions in which there are differences between H-ras GTP and H-ras GDP in loop 2. The term "GTP extended" denotes the residue which has an extended form in the H-ras GTP complex. In the case of "wound", the residues have wound forms. In the case of "intermediate", the residues have "intermediate" forms. In the case of "not determined", the form of the residue is not determined.

In the paper of Kobayashi *et al.* [44], in the loop 4 region, the conformation differences between H-ras GTP and H-ras GDP lead to the differences of the dihedral angles of the backbone ALA59-SER65 residues. In the H-ras GTP complex, in loop 4, the residues other than ALA59 and GLU61 had wound forms. In the H-ras GDP complex, ALA59-GLU62 had extended forms as well as wound forms, although the GLU63-SER65 had stable extended forms.

In our results, in the loop 4 region, the conformation differences between H-ras GTP and H-ras GDP lead to the differences of the dihedral angles of the backbone residues ALA59, GLN61-GLU63 and ALA66-ARG68. In the H-ras GTP complex, the GLU63 residue has an extended form, residues GLU62 and ALA66-ARG68 have the wound form, and the dihedral angles of residues ALA59 and GLN61 are not determined. In the H-ras GDP complex, residues ALA59, GLN61, GLU62, ALA66 and MET67 have the extended form, and residues GLU63 and ARG68 have the intermediate form.

The reasons of the differences between the results of Kobayashi *et al.* [44] and our results arise from using the different initial structures and using the different parameters in force field. They used PDBID:5P21 for the H-ras GTP complex and PDBID:4Q21 for the H-ras GDP complex, although we use PDBID:121P for the H-ras GTP and PDBID:1Q21 for the H-ras GDP.

They used the parameters for guanine nucleotides determined by Meagher *et al.* [45], in which the parameters of the GTP-protein complex and of the GDP-protein complex were not calculated directly. The force fields and the charges around Mg^{2+} were not discussed in their papers. We calculated the atomic charges of guanine nucleotides determined in the H-ras GTP complex and in the H-ras GDP complex. And we calculated the bond parameters K_{b} and the angle parameters K_θ in the H-ras GTP complex and in the H-ras GDP complex.

2.4 Conclusions

Our calculation shows that the oxygen atoms in the GTP or GDP bind tightly to the Mg^{2+} although the ones in the H_2O bind loosely. The value of charges of some phosphates of GTP or GDP are improved by using a basis functional set 6-31G**. Our calculations of the molecular orbitals suggest that the γ-phosphate of GTP has a nucleophilic property.

We performed MD simulations of H-ras GTP complex and H-ras GDP complex using the parameter set obtained in this chapter. The structure differences between the H-ras GTP complex and H-ras GDP were found in

the loop 2 and loop 4 mainly. We checked the validity of these potential parameters by comparing results of these simulations with results of Kobayashi *et al.* [44].

In our future works, we will perform MD simulations for longer time and calculate the free energy difference between the H-ras GTP complex state and H-ras GDP complex state. We will check if the dihedral term is small enough in Mg-subsystem. Furthermore, using the same methods as in this chapter, we would like to investigate the properties of the complexes of the H-ras mutants or Mras mutants and GppNHp or GTPγS, which are considered to have the structures of intermediate states of GTP hydrolysis in the H-ras GTP complex [51], we can perform MD simulations of the intermediate states of GTP hydrolysis in the H-ras GTP complex.

Chapter 3

Molecular Dynamics Simulations of the Hras GTP and GDP Complexes

We study the structures of the Hras-GTP complex and the Hras-GDP complex in water in order to investigate the mechanism of GTP hydrolysis of the Hras-GTP complex. We performed MD simulations of the Hras-GTP complex and the Hras-GDP complex in water in order to investigate the structures of these complexes using the potential parameters of AMBER ff03 and our parameters around Mg^{2+}. Our simulations show that the averaged

structure differs between the Hras-GTP complex and Hras-GDP complex are found in the Switch I and II regions. Especially in the Switch II region, the $\alpha 2-$helix of Hras-GDP is shorter than the $\alpha 2-$helix of Hras-GTP. The water molecules around GTP and GDP stay for a longer time than the diffusion of ordinary water molecules.

3.1 Introduction

Guanine nucleotide binding proteins (G-proteins) are included in many cell processes such as signal transduction, transportation and secretion of proteins and elongation of polypeptides. Every G-protein acts as a molecular switch. In active state, a G-protein forms a complex with GTP; in inactive state a G-protein forms a complex with GTP. Hras is one of G-proteins.

Hras is a product of proto-oncogene *Hras*, and is included in the signaling process to induce the cell growth. A certain activated mutation of Hras, observed frequently in various types of tumor, leads to continuous signaling to downstream elements [28]. To understand the mechanism of GTP hydrolysis in H-ras, it is crucial to know the structures of Hras-GTP complex and Hras-GDP complex in solution. The crystal structures of the Hras-GTP

complex [29] and the Hras-GDP complex [30] have been studied by x-ray crystallographic analyses.

In order to sample the structures of Hras-GTP complex and Hras-GDP complex in water solution, the molecular dynamics (MD) simulations have been performed in several studies [39, 41–44]. In this chapter, we show our results of our MD simulations. We need force fields of atoms in order to perform MD simulations. We use the AMBER ff03 fields [38] for most atoms. However, the following two kinds of parameters were not given in AMBER ff03; (1) atomic charges for Mg^{2+} and GTP/GDP and residues which binds to Mg^{2+} coordinately, (2) the force strength between Mg^{2+} and oxygen atoms which bind to Mg^{2+} coordinately. We calculated these parameters in our previous work [52]. We use these parameters and performed MD simulations in this chapter.

3.2 Methods

All of the MD simulations described in this chapter were performed by AMBER 11 program [48]. We used the AMBER ff03 for most of proteins and for most of ions, and used TIP3P [49] for water molecules. We used our cal-

culated parameters [52] for Mg^{2+}, GTP, GDP and residues including oxygen atoms which bind to Mg^{2+} coordinately, as mentioned in Introduction.

In order to model the initial state of GTP, we use the structure determined by x-ray PDBID:121P.

First, because GCP, which is a slowly hydrolyzable GTP analogue, was used in the x-ray analysis of the structure of 121P, we start with GCP and substitute the C atom in GCP to the O atom in order to change GCP to GTP.

Secondly, we add the TIP3P water molecules to the system. In order to neutralize the charge of systems, counterions are added. The SHAKE algorithm is used for bonds which include hydrogen atom. We minimize the energy of the system of Hras-GTP complex and water by using the steepest descent method. Next, we heat the temperature of water molecules in water solution to 300K under NPT conditions, while we restrict the positions of the Hras-GTP complex and water molecules of crystallization by harmonic potentials with strength 50 kcal/mol. At 300K temperature, we gradually remove the above restriction. We perform equilibration simulation for 50 ps. We use the Langevin thermostat for temperature coupling. We use the pressure coupling algorithm of weak-coupling, provided in AMBER, which

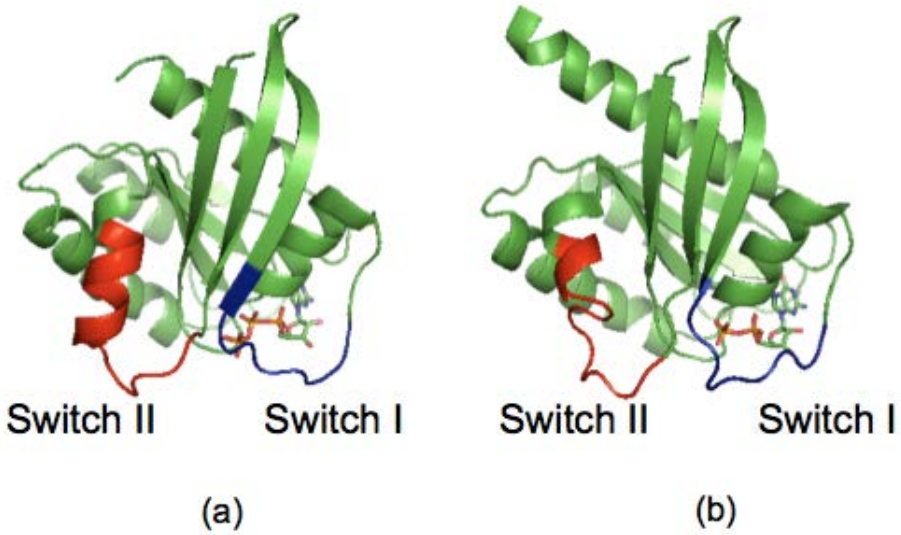

Figure 3.1: The structure of the switch regions in the Hras-GTP complex (a) and in the Hras-GDP complex (b). The figures are drawn using the PDBID:121P (a) and PDBID:1Q21 (b). In (a), we substituted GTP in place of GCP in PDBID:121P.

is analogous to temperature coupling [50]. The time constant of pressure coupling with bath is 1 ps. Time step of equilibration and MD simulations is 1 fs.

Fig. 3.1 shows the switch regions in the Hras-GTP complex (a) and in the Hras-GDP complex (b). Differences of structures between the Hras-GTP complex and the Hras-GDP complex are in the switch I region and in the switch II region. The switch I region includes 30-38 residues, which form loop 2 and a part of $\beta 2$ strand. The switch II region includes 60-72 residues,

which form loop 4 and $\alpha 2$ helix.

The conformational changes mentioned above have been known to result from the fact that Thr35 binds coordinately to Mg^{2+} in Hras-GTP complex while Thr35 does not bind in Hras-GDP complex [31–37].

3.3 Results

Fig. 3.2 shows the structure after equilibration, described in the Methods, of the Hras-GTP complex (a) and the Hras-GDP complex (b). The arrows indicate the main difference between the Hras-GTP complex and the Hras-GDP complex. The $\alpha-$helices presented in the Hras-GTP change to coils in the Hras-GDP complex.

Fig. 3.3 shows root mean square of deviation of C_α of Hras from the start of the MD simulation in the Hras-GTP complex (a) and in the Hras-GDP complex (b). The value of RMSD changes moderately after the MD simulation of 11 ns, in both cases of the Hras-GTP and the Hras-GDP. This suggests that each system reached the state appropriate to be sampled.

Fig. 3.4 shows averaged structures of the switch regions of the Hras-GTP complex (a) and of the Hras-GDP complex (b). Arrows indicate locations

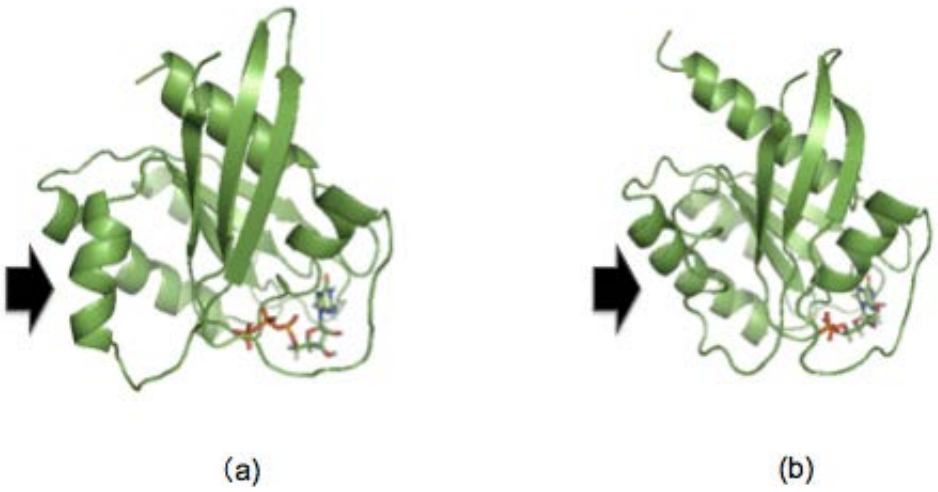

Figure 3.2: Structure after equilibration of the Hras-GTP complex (a) and the Hras-GDP complex (b). The arrows indicate the locations of the main difference between the Hras-GTP complex and the Hras-GDP complex.

of the main difference of structures between the Hras-GTP complex and the Hras-GDP complex. The $\alpha-$helices are long in the the Hras-GTP complex, although the $\alpha-$helices are short in the the Hras-GDP complex.

Fig. 3.5 shows root mean square of fluctuation of C_α of Hras in the Hras-GTP complex and in the Hras-GDP complex in the switch I region (a) and in the switch II region (b). From Fig. 3.5(a) we find that the fluctuation of Thr35 in the Hras-GDP complex is larger than the fluctuation of Thr35 in the Hras-GTP complex. This is because Thr35 in the Hras-GTP complex binds to Mg^{2+} coordinately, while Thr35 in the Hras-GDP complex does not

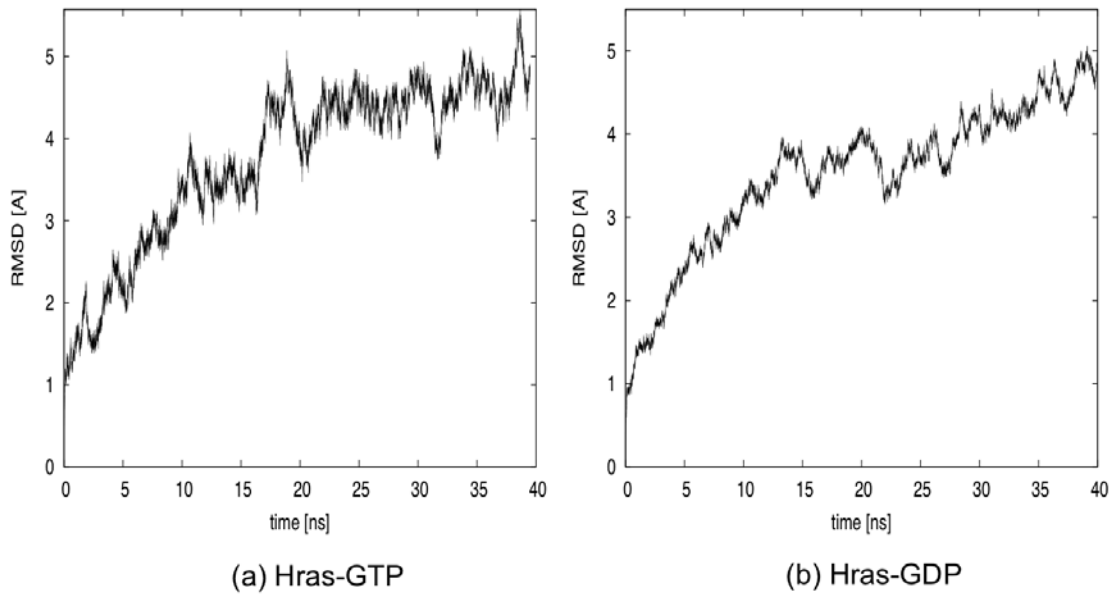

Figure 3.3: Root mean square of deviation of C_α of Hras from the start of the MD simulation in the Hras-GTP complex (a) and in the Hras-GDP complex (b).

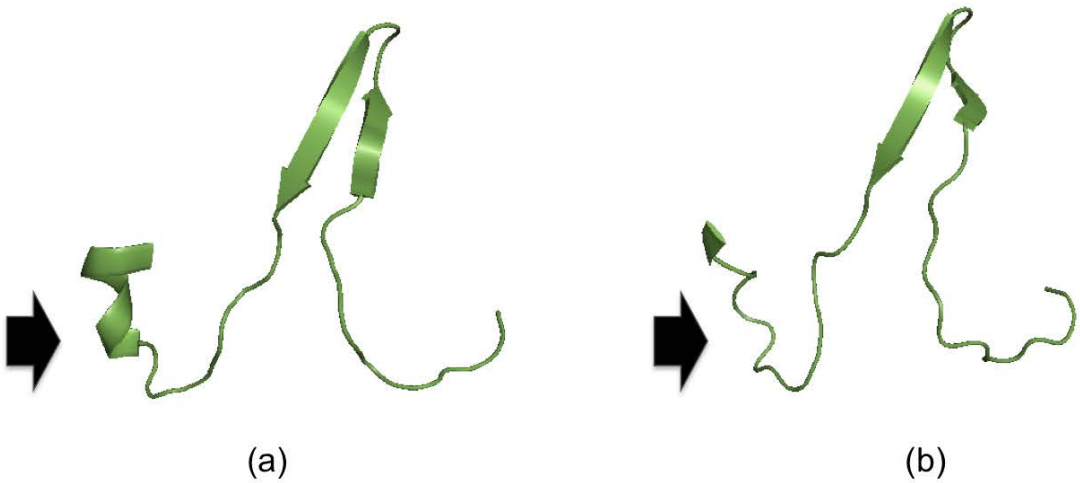

Figure 3.4: Averaged structures of the switch regions of the Hras-GTP complex (a) and of the Hras-GDP complex (b). Arrows indicate the location of the main difference of structures between the Hras-GTP complex and the Hras-GDP complex.

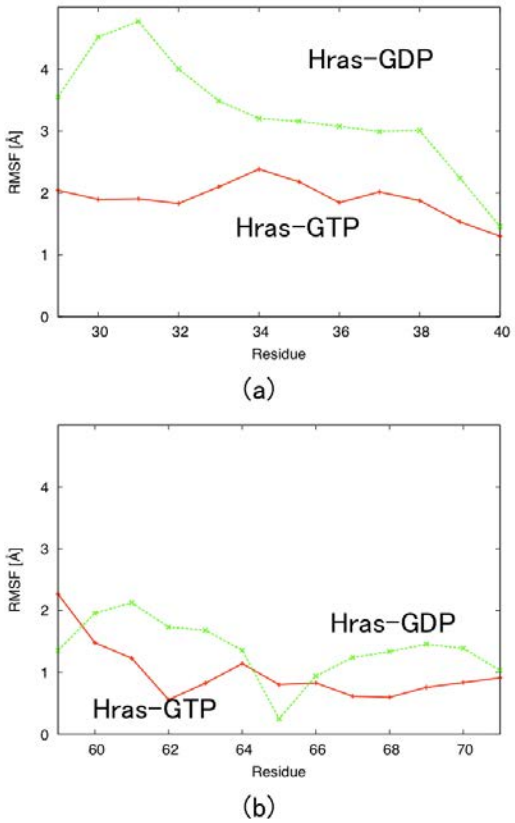

Figure 3.5: Root mean square of fluctuation of C_α of Hras in the Hras-GTP complex (red solid line) and in the Hras-GDP complex (green dashed line) in the switch I region (a) and in the switch II region (b).

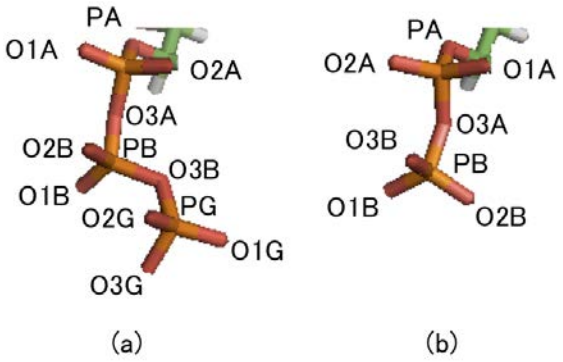

Figure 3.6: The phosphorus atoms and the oxygen atoms in the phosphate groups of GTP (a) and GDP (b).

bind to Mg^{2+} coordinately.

Fig. 3.6 shows the phosphorus atoms and the oxygen atoms in the phosphate groups of GTP or GDP.

Fig. 3.7 shows radial distribution functions (RDF) of oxygen atoms in H_2O with respect to the phosphorus atoms in GTP (a) and GDP (b). In Fig. 3.7 (a), red lines describe the H_2O around PA, green lines describe the H_2O around PB, and blue lines describe the H_2O around PG. We found that the radius of the first hydration sphere is 4.66 Å for PA, 4.91 Å for PB and 4.77 Å for PG.

Because the first peak for PA is the largest, we can predict that the number of water is the largest for PA. In detail, we need to compare the integrated values of $4\rho\pi g(r)r^2$ in the first hydration sphere, where ρ is the

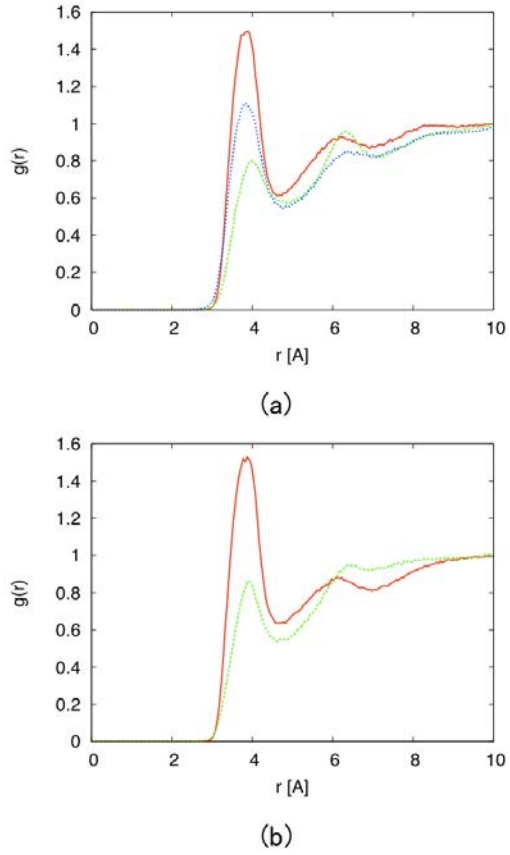

Figure 3.7: Radial distribution functions of oxygen atoms in H_2O with respect to the phosphorus atoms in GTP (a) and GDP (b). Red lines describe the H_2O around PA, green lines describe the H_2O around PB, and blue lines describe the H_2O around PG.

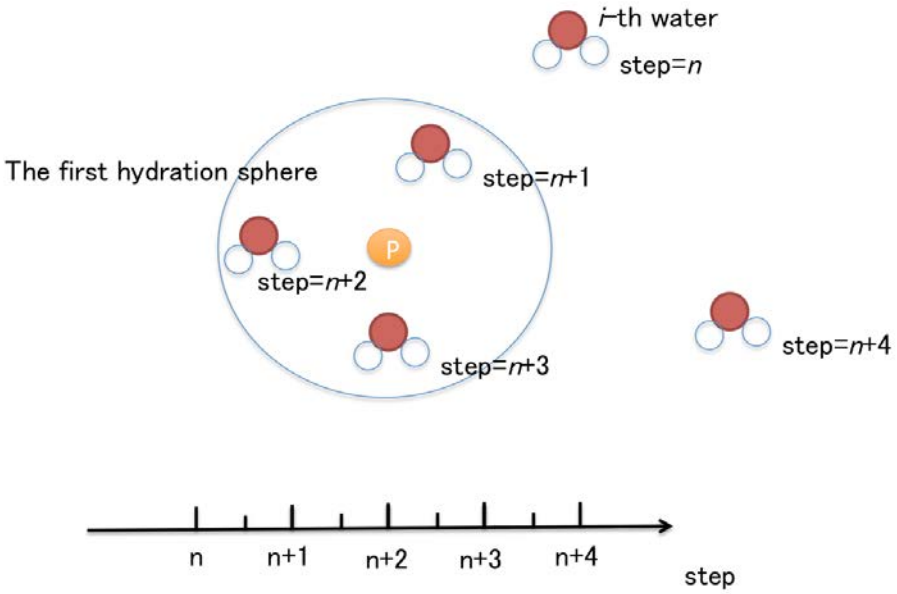

Figure 3.8: The schematic explanation of the method to estimate the duration time of water molecules around the guanine nucleotide from the MD simulation trajectories.

number density of water molecules. The number of water molecules in the first sphere is 1.32 for PA, 0.96 for PB and 1.23 for PG.

From Fig. 3.7. (b), we found that the radius of the first hydration sphere is 4.66 Å for PA and 4.66 Å for PB. The number of water molecules in the first sphere is 3.88 for PA and 2.15 for PB.

We calculated the duration time of water molecules around the guanine nucleotide from the MD simulation trajectories. Fig. 3.8 shows the schematic explanation of method to estimate the duration time. For example, we can

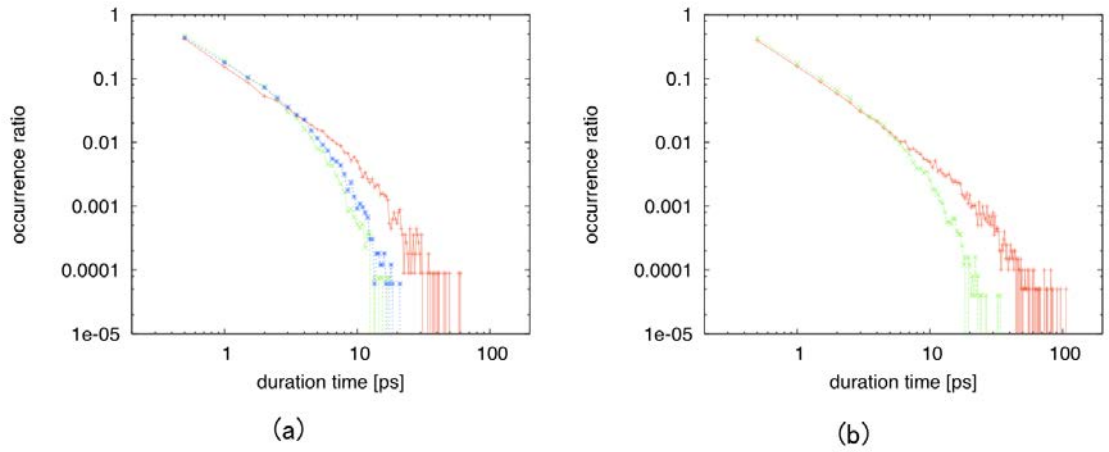

Figure 3.9: Occurrence ratio distribution of the duration time in the first hydration sphere of phosphorus atom in GTP (a) and in GDP (b). The red mark is for PA, the green mark is for PB, and the blue mark is for PG.

follow the trajectory of the i-th water molecules in a MD simulation. We assume the case that the n-th snap shot of trajectory of the i-th water is out of the first hydration sphere, and the $(n+1)$, $(n+2)$ and $(n+3)$-th snap shots are in the first hydration sphere, and $(n+4)$-th snap shot is out of the first hydration sphere. We cannot determine exactly the correct time of entry and exit of water molecules in the first hydration sphere. So we estimate this as the half of the time interval of snap shots of MD trajectories $\Delta_{\mathrm{snap\_shot}}$. In the assumed case described above, the duration time is estimated as $((n+3.5)-(n+0.5))\Delta_{\mathrm{snap\_shot}}$.

Fig. 3.9 shows occurrence ratio distribution of the duration time in the

oxygen atom in H_2O in the first hydration sphere of phosphorus atom in GTP (a) and in GDP (b). In Fig. 3.9, the horizontal axis is the duration time estimated as shown in Fig. 3.8, and the vertical axis is the frequency of occurrence, the summation of these are normalize to 1, so we call it the occurrence ratio. For example, duration time of 1 ps was found in 0.1 (10 %) of the total time. Most of lines coincide for small duration time. These lines are nearly proportional to $t^{-1.4}$ for small duration time for PA in GTP and PA and PB in GDP. These lines are nearly proportional to $t^{-1.3}$ for small duration time for PB and PG in GTP. This suggests that water molecules around guanine nucleotide stay for a longer time than ordinary diffusion. The curves of PA have longer tail than curves of PB and PG, in both cases of GTP and GDP.

3.4 Summary

We studied the structures of the Hras-GTP complex and the Hras-GDP complex in water in order to investigate the mechanism of GTP hydrolysis of the Hras-GTP complex. We performed MD simulations of the Hras-GTP complex and the Hras-GDP complex in water in order to investigate the

structures of these complexes using the potential parameters of AMBER ff03 and our parameters around Mg^{2+}. Our simulations show that the differences of averaged structure between the Hras-GTP complex and Hras-GDP complex are found in the Switch I and II regions. Especially in the Switch II region, the $\alpha 2-$helix of Hras-GDP is shorter than the $\alpha 2-$helix of Hras-GTP. The water molecules around GTP and GDP stay for a longer time than the diffusion of ordinary water molecules.

Chapter 4

Discussion

In this chapter, we discuss the results obtained from our calculations and our simulations.

4.1 Calculations of potential parameters

4.1.1 Atomic charge

The difference of the atomic charges between Hras GTP and Hras GDP is largest for O3B. In the Hras GTP complex, the O3B atom belongs to the inner phosphate group and does not bind to Mg^{2+}. In the Hras GDP complex, the O3B atom belongs to the outer phosphate group and binds to

Mg^{2+} coordinately.

The atomic charge of Mg^{2+} in the Hras GTP complex is +1.037 and the atomic charge of Mg^{2+} in the Hras GDP complex is +1.297 by the influence of the coordinate bonds by six oxygen atoms. The difference is caused by the group or molecule where the oxygen atoms belong. The Mg^{2+} ion in the Hras GTP complex binds to six oxygen atoms: two oxygens in GTP, two oxygens in amino acid residues and two oxygens in H_2Os. The Mg^{2+} ion in the Hras GDP complex binds to six oxygen atoms: one oxygen in GDP, one oxygen in amino acid residue and four oxygens in H_2Os. As shown in Table 2.2, the oxygen atoms of H_2O bind to Mg^{2+} more weakly than the oxygen atoms of guanine nucleotide or the oxygen atoms of amino acid residues.

OW (oxygen in water) of H_2O172 in the Hras GTP complex and OW of H_2O201 in the Hras GDP complex have larger negative charges than that of TIP3P model (-0.834), although OWs of other H_2O molecules have almost the same negative charge as TIP3P model. Those are caused by the anisotropy of the electric fields around Mg^{2+} in direction, since distances of OWs in H_2Os to Mg^{2+} are almost the same.

The difference between our calculated value and the value calculated by Worth *et al.* [41] in Hras GTP complex is large for PA, O1G and PB. This

difference is caused by the difference in the number of the basis set and in the number of polarized functions of the basis set. The difference between our calculated value and the value calculated by Worth *et al.* [41] in Hras GDP complex is large for PB, O3A and PA. This difference is caused by the reasons mentioned in the case of Hras GTP complex.

In fact, in the calculation by Worth *et al.* [41], they used the spread wave functions. Since GTP and GDP have large negative charge, it will be interesting to use the spread wave functions in the future.

4.1.2 Force parameters

In the Hras GTP complex, the oxygen atoms of GTP bind tightly to Mg^{2+}, although the oxygen atoms of H_2O bind loosely to Mg^{2+}. In the Hras GDP complex, the oxygen atoms of GTP or SER17 bind tightly to Mg^{2+}, although the oxygen atoms of H_2O bind loosely to Mg^{2+}.

The strength of binding of GTPO2B to Mg^{2+} in the Hras GTP complex is almost the same as the strength of binding of GTPO3B to Mg^{2+} in the Hras GDP complex. Both of the atoms belong to the most outside phosphate group of the guanine nucleotide, and bind to Mg^{2+} coordinately. The strength of binding of SER17OG to Mg^{2+} in the Hras GTP complex is almost the same

as the strength of binding of SER17OG to Mg^{2+} in the Hras GDP complex. From this fact, the shapes of the backbone near SER17 in the Hras GTP complex and in the Hras GDP complex are almost the same. We assume that the most important parts of the potentials are the bond part and the angle part. The dihedral angle parts containing Mg^{2+} ion are not considered. In the future, it will be interesting to include the dihedral parts restricting the rotation around the Mg^{2+}-O axis.

4.2 Estimation of chemical reactions from the Kohn-Sham orbitals

As shown in Fig. 2.5 (a) and (b), the HOMO (highest occupied molecular orbitals) of Hras GTP complex is spread widely at O1, O2 and O3 of γ phosphate of GTP, although the LUMO (lowest unoccupied molecular orbitals) shrinks at O1 and O3 of γ phosphate of GTP. These suggest that electrophiles attack the area of O1, O2 and O3 of γ phosphate of GTP, because the electronic density of HOMO is high at O1, O2 and O3 of γ phosphate of GTP.

As shown in Fig. 2.5 (c) and (d), the HOMO of Hras GDP complex is dominant around O1, O2 and O3 of β phosphate of GDP, although the

LUMO is dominant in the area between H_2O202, H_2O203 and H_2O204. These suggest that electrophiles attack the area of O1, O2 and O3 of β phosphate of GDP, because the electronic density of HOMO is high at O1, O2 and O2 of β phosphate of GDP. These also suggest that nucleophiles attack the area between H_2O202, H_2O203 and H_2O204, because the electronic density of LUMO is high in the area between H_2O202, H_2O203 and H_2O204.

4.3 Conformation in MD simulations

4.3.1 Averaged structures

The averaged structures of Hras GTP complex and Hras GDP complex have the similar shape. The main parts of structures, which are different between the Hras GTP complex and Hras GDP complex, are switch I and switch II regions.

4.3.2 Backbone Dihedral angles

We calculate the dihedral angles of backbone of Hras GTP complex and Hras GDP complex. Comparing the results of Hras GTP and the results of Hras GDP in the switch I region and switch II region, the main difference is found

in the residue of 66-68, which corresponds to the part of the α_2 helix near the loop4.

4.3.3 RMSFs

We calculate the root mean square of fluctuations (RMSF) from the principal coordinate analysis of the simulations of Hras GTP complex and Hras GDP complex. Comparing the results of Hras GTP and the results of Hras GDP in the switch I region and switch II region, the main difference is found in the residue THR35: THR35 binds to Mg^{2+} coordinately in the Hras GTP complex while THR35 does not bind to Mg^{2+} in the Hras GDP complex.

4.4 Properties of the water molecules near the guanine nucleotide

We calculated the radial distribution functions (RDF) of water molecules around the phosphorus atoms of guanine nucleotide nucleotide in the Hras GTP complex and GDP complex. We define the radius of the first hydration sphere from the first peak of RDF.

4.4.1 RDF and the radius of the first hydration sphere

We calculated the radial distribution functions of water molecules around the phosphorus atoms of GTP in the Hras GTP complex. We find that the radius of the first hydration sphere is 4.66Å for PA, 4.91Å for PB and 4.77Å for PG.

We calculated the radial distribution functions of water molecules around the phosphorus atoms of GDP in the Hras GDP complex. We find that the radius of the first hydration sphere is 4.66Å for PA and 4.66Å for PB.

4.4.2 Number of water molecules in the first hydration sphere

We calculated the averaged number of water molecules in the first hydration sphere around the phosphorus atoms of GTP in the Hras GTP complex. The number of water molecules is 1.32, 0.96 and 1.23 for PA, PB and PG.

We calculated the averaged number of water molecules in the first hydration sphere around the phosphorus atoms of GDP in the Hras GDP complex. The numbers of water molecules is 3.88 and 2.15 for PA and PB.

4.4.3 Duration time of the first hydration sphere

We calculated the distribution of the duration time of water molecules in the first hydration sphere around the phosphorus atoms of GTP in the Hras GTP complex. We find that the curves of the distribution of the duration time are proportional to $t^{-1.4}$ for PA and are proportional to $t^{-1.3}$ for PB and PG, for the short duration time.

We calculated the distribution of the duration time of water molecules in the first hydration sphere around the phosphorus atoms of GDP in the Hras GDP complex. We find that the curves of the distribution of the duration time are proportional to $t^{-1.4}$ for PA and PB, for the short duration time.

Chapter 5

Conclusion

We investigated the properties of the atoms around the Mg^{2+} in the Hras GTP complex and in the Hras GDP complex by the quantum chemical calculations and by the molecular dynamics simulations. We used all-atom model to study the Hras GTP complex and the Hras GDP complex. We obtained the following conclusions.

5.1 Calculations of potential parameters

We calculated the potential parameters in the Hras GTP complex and in the Hras GDP complex. We found that the oxygen atoms in the GTP or GDP bind tightly to the Mg^{2+} although the ones in the H2O bind loosely. The

values of charges of some phosphates of GTP or GDP are improved by using a basis functional set 6-31G**.

5.2 Estimation of chemical reactions from the Kohn-Sham orbitals

When we calculated the potential parameters, we also calculated the Kohn-Sham orbitals in the Hras GTP complex and in the Hras GDP complex. Our calculations of the Kohn-Sham orbitals suggest that the γ-phosphate of GTP has a nucleophilic property.

5.3 Molecular dynamics simulations

We performed MD simulations of H-ras GTP complex and H-ras GDP complex using the parameter set obtained by our quantum calculations. The structure difference between the H-ras GTP complex and H-ras GDP was found in the loop 2 and loop 4 mainly. We checked the validity of these potential parameters by comparing results of these simulations with results of Kobayashi *et al.* [44].

We also investigate the properties of water molecules near the guanine nucleotide in the Hras GTP complex and GDP complex. We found that the total hydration numbers of the phosphorus atoms near GDP is larger than those near GTP, and the hydration numbers of each phosphorus atom near GDP is larger than those near GTP. The occurrence ratio distribution of the duration time in the first hydration sphere of GTP or GDP is proportional to $t^{-1.4}$. These suggest that the water molecules stay near the guanine nucleotide for a longer time than the water molecules with the ordinary diffusion.

5.4 Future work

Following the investigation described in this thesis, we have two directions of research for the understanding of the mechanism of GTP hydrolysis in the H-ras GTP complex.

One direction of research is the progress of investigation of the properties of water molecules around GTP or GDP. X. Du *et al.* summarized the candidates of the mechanism of the hydrolysis of GTP in the Hras GTP hydrolysis described in Fig. 5.1 [53]. We should estimate the angular distribution of

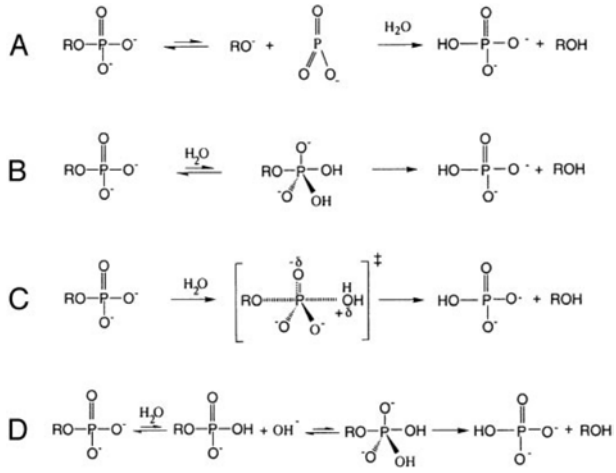

Figure 5.1: The candidates of the mechanism of the hydrolysis of GTP in the Hras GTP hydrolysis summarized by X. Du *et al.* [53]. Dissociative (A) and associative (B) mechanistic extremes, the concerted pathway (C), and the substrate-assisted mechanism (D) are shown.

the positions of water molecules in order to know if the mechanism of GTP hydrolysis is dissociative denoted as (A) in Fig. 5.1. For example, when we estimate the angular distribution of the positions of water molecules around PG atom in GTP, we will set the axes of coordinates as the following. First, we set PG as the origin. Next, we set the O3B-PG line as the z-axis. We then obtain a plane which contains PG and which is perpendicular to O3B-PG. We project the line segment PG-O1G onto this plane. We choose the x-axis along this projected line segment. The position of a water molecule in the coordinates is shown in Fig. 5.2. If the mechanism of GTP hydrolysis is

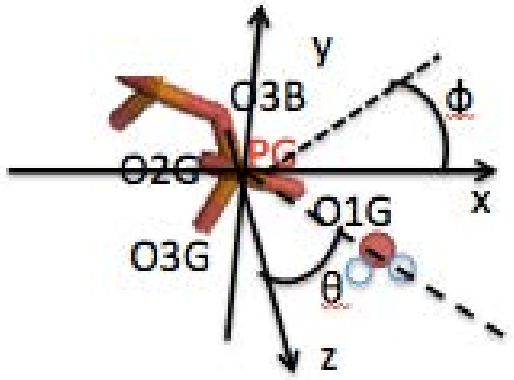

Figure 5.2: An example of axes of coordinates around PG. These axes of coordinates are used in order to estimate the angular distribution of positions of water molecules around PG.

dissociative, the attacking water molecule attacks to $\gamma-$phosphate of GTP along with O3B-PG axis. In this scenario, the angular distribution of the water molecules must be high at the O3B-PG axis. If the angular distribution of the water molecules is not so high at the O3B-PG axis, the mechanism of GTP hydrolysis is not dissociative. Thus, the mechanism of GTP hydrolysis should be one of the mechanism: 1. associative, 2. mechanistic extremes, 3. the concerted pathway, and 4. the substrate-assisted mechanism. Those four types of mechanism have the associative transition state.

The second direction of research is the application of the solvation free energy to the Hras-GTP complex and Hras-GDP complex. Ordinary application of the solvation free energy to estimate the binding free energy is

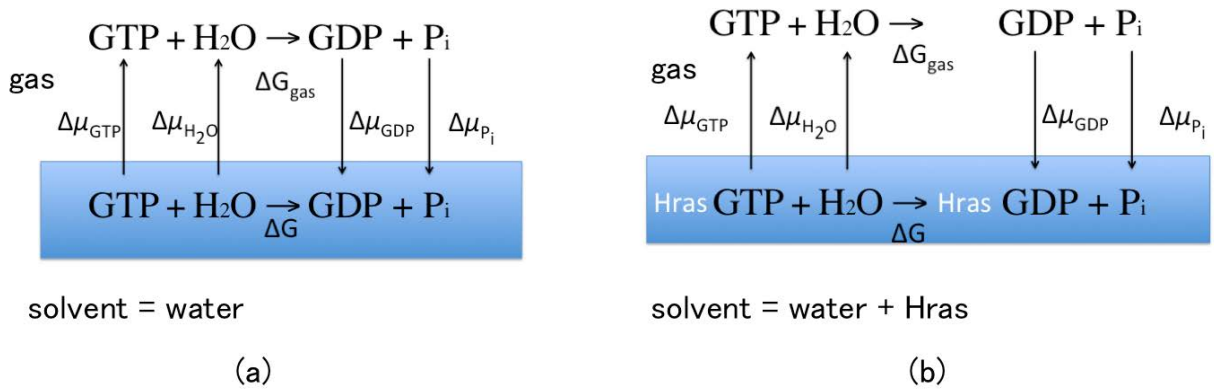

Figure 5.3: The solvation free energy to estimate the binding free energy is in the gas environment and in the water solvation environment (a). The solvation free energy to estimate the binding free energy is in the gas environment and in the solvent consisting of water and protein (b).

in the gas environment and in the water solvation environment shown in Fig. 5.3(a). Interaction between water and GTP (or GDP) is integrated in thermodynamic integration in order to estimate the binding free energy as follows:

$$\int_0^1 \mathrm{d}\lambda \frac{\partial V}{\partial \lambda}, \tag{5.1}$$

where λ is the parameter of interaction strength, and V is the interaction between water and GTP (or GDP). In the modified application of the solvation free energy, water and protein are regarded as the solvent shown in Fig. 5.3(b). Interaction between water and GTP (or GDP) and interaction between protein and GTP (or GDP) are integrated in thermodynamic in-

tegration in order to estimate the binding free energy. The free energy of reactions in the solvent is estimated.

Further application in the second direction of research is the application of the method estimating the free energy of reactions to estimating the free energy of activation. This is achieved by replacing the GDP to the candidates of the guanine nucleotide in transition states. The mechanism of hydrolysis of GTP in Hras GTP complex will be clear by comparing the results of possible candidates.

List of publications

Papers as first author

(1). T. Miyakawa, R. Morikawa, M. Takasu, K. Sugimori, K. Kawaguchi, H. Saito, and H. Nagao, *The Potentials of the Atoms around Mg2+ in the H-ras GTP and GDP Complexes*, Progress in Theoretical Chemistry and Physics, accepted (2012).

(2). T. Miyakawa, R. Morikawa, M. Takasu, K. Sugimori, T. Mizukami, K. Kawaguchi, H. Saito and H. Nagao, *Molecular Dynamics Simulations of the Hras-GTP complex and the Hras-GDP complex*, International Journal of Quantum Chemistry, submitted.

Other papers

(1). S. Kawamoto, M. Takasu, T. Miyakawa, R. Morikawa, T. Oda, S. Futaki and H. Nagao, *Inverted micelle formation of cell-penetrating peptide studied by coarse-grained simulation: Importance of attractive force between cell-penetrating peptides and lipid head group*, Journal of Chemical Physics, 134, 095103 (2011).

(2). H. Yamada, Y. Komatsu, T. Miyakawa, R. Morikawa, F. Katagiri, K. Hozumi, Y. Kikkawa, M. Nomizu and M. Takasu, *Conformation Analysis of Loop Region Peptides in the Laminin Alpha Chain LG4 Modules by Molecular Dynamics Simulations*, Peptide Science, Japan Peptide Society, 201 (2011).

(3). S. Kawamoto, M. Takasu, T. Miyakawa, R. Morikawa, T. Oda, S. Futaki and H. Nagao, *Binding of Tat peptides on DOPC and DOPG lipid bilayer membrane studied by molecular dynamics simulations*, Molecular Simulation, 38, 366 (2012).

(4). H. Saito, T. Mizukami, S. Kawamoto, T. Miyakawa, M. Iwayama, M. Takasu and H. Nagao, *Molecular Dynamics Studies of Lipid Bilayer with Gramicidin A: Effects of Gramicidin A on Membrane Structure*

and Hydrophobic Match, International Journal of Quantum Chemistry, 112, 161 (2012).

(5). S. Kawamoto, T. Miyakawa, M. Takasu, R. Morikawa, T. Oda, H. Saito, S. Futaki and H. Nagao, *Cell Penetrating Peptide Induces Various Deformations of Lipid Bilayer Membrane: Inverted Micelle, Double Bilayer and Trans-membrane*, International Journal of Quantum Chemistry, 112, 178 (2012).

(6). T. Mizukami, H. Saito, S. Kawamoto, T. Miyakawa, M. Iwayama, M. Takasu and H. Nagao, *Solvation Effect of the Structural Change of a Globular Protein: a Molecular Dynamics Study*, International Journal of Quantum Chemistry, 112, 344 (2012).

(7). K. Fujiwara, K. Horiuchi, S. Goryoda, Y. Hashidume, N. Horiguchi, T. Miyakawa, M. Takasu and M. Aoki, *Observation of Cell-Size Variation under Environmental Stress by Fluorescence Correlation Spectroscopy without Objective Image Magnification*, Journal of Environmental Science and Engineering (A & B), 1, 364 (2012).

Bibliography

[1] B. Alberts, A. Johnson, J. Lewis, M. Raff, K. Robertss, and P. Walter, *Molecular Biology of the Cell 5th Edition*, Garland, 2002.

[2] B. J. Alder and T. E. Wainwright, *J. Chem. Phys.*, **27**, 1208, 1957.

[3] A. Rahman, *Phys. Rev.*, **136**, A405–A411, 1964.

[4] A. Rahman and F. H. Stillinger, *J. Chem. Phys.*, **55**, 3336, 1971.

[5] J-P. Ryckaert, G. Ciccotti, and H. J. C. Berendsen, *J. Comput. Phys.*, **23**, 327–341, 1977.

[6] J. A. McCammon, B. R. Gelin, and M. Karplus, *Nature*, **267**, 585, 1977.

[7] H. C. Andersen, *J. Chem. Phys.*, **72**, 2384–2393, 1980.

[8] M. Parinello and A. Rahman, *J. Appl. Phys*, **52**, 7182, 1981.

[9] S. Nosé, *J. Chem. Phys.*, **81**, 511–519, 1984.

[10] W. L. Jorgensen and J. Tirado-Rives, *J. Am. Chem. Soc.*, **110**, 1657–1666, 1988.

[11] M. Saito, *Kagaku*, **61**, 822, 1991.

[12] C. Chothia, *Nature*, **248**, 338, 1974.

[13] T. Ooi, M. Oobatake, G. Némethy, and H. A. Scheraga, *Proc. Natl. Acad. Sci. USA*, **84**, 3086, 1987.

[14] R. Constanciel and R. Contreras, *Theor. Chim. Acta*, **65**, 1, 1984.

[15] W. C. Still, A. Tempczyk, R. C. Hawley, and T. Hendrickson, *J. Am. Chem. Soc.*, **112**, 6127–6129, 1990.

[16] D. Bashford and D. A. Case, *Annu. Rev. Phys. Chem.*, **51**, 129, 2000.

[17] Y. S. Watabnabe, J. G. Kim, Y. Fukunishi, and H. Nakamura, *Chem. Phys. Lett.*, **400**, 258, 2004.

[18] August Wilhelm von Hofmann, His public lectures, 1860.

[19] Jacobus Henricus van't Hoff, *La chimie dans l'espace*, 1874.

[20] Donald H. Andrews, *Phys. Rev.*, **36**, 544–554, 1930.

[21] F. H. Westheimer and Joseph E. Mayer, *J. Chem. Phys.*, **14**, 733, 1946.

[22] J. B. Hendrickson, *J. Am. Chem. Soc.*, **83**, 4537–4547, 1961.

[23] K. B. Wiberg, *J. Am. Chem. Soc.*, **87**, 1070–1078, 1965.

[24] P. De Santis, E. Giglio, A. M. Liquori, and A. Ripamonti, *J. Pol. Sci. Part A*, **1**, 1383–1404, 1963.

[25] D. A. Brant and P. J. Flory, *J. Am. Chem. Soc.*, **87**, 2791–2800, 1965.

[26] N. L. Allinger, M. T. Tribble, M. A. Miller, and D. H. Wertz, *J. Am. Chem. Soc.*, **93**, 1637–1648, 1971.

[27] Wikipedia, Wikipedia, the free encyclopedia, 2012, [Online; accessed June-2012].

[28] J. Downward, *Nat. Rev. Cancer*, **3**, 11–22, 2003.

[29] E. F. Pai, U. Krengel, G. A. Petsko, R. S. Goody, W. Kabsch, and A. Wittinghofer, *EMBO J.*, **9**, 2351–2359, 1990.

[30] M. V. Milburn, L. Tong, A. M. deVos, A. Brünger, Z. Yamaizumi, S. Nishimura, and S. H. Kim, *Science*, **247**, 939–945, 1990.

[31] M. A White, C. Nicolette, A. Minden, A. Polverino, V. A. Linda, M. Karin, and M. H. Wigler, *Cell*, **80**, 533–541, 1995.

[32] Y. J. Sung, M. Carter, J. M. Zhong, and Y. W. Hwang, *Biochemistry*, **34**, 3470–3477, 1995.

[33] M. C. C. Hwang, Y. J. Sung, and Y. W. Hwang, *J. Biol. Chem.*, **271**, 8196–8202, 1996.

[34] P. Rodriguez-Viciana, P. H. Warne, A. Khwaja, B. M. Marte, D. Pappin, P. Das, M. D. Waterfield, A. Ridley, and J. Dowanward, *Cell*, **89**, 457–467, 1997.

[35] M. Spoerner, C. Herrmann, I. R. Vetter, H. R. Kalbitzer, and A. Wittinghofer, *Proc. Natl. Acad. Sci. USA.*, **98**, 4944–4949, 2001.

[36] J. J. Fiordalisi, S. P. Holly, R. L. Johnson II, L. V. Parise, and A. D. Cox, *J. Biol. Chem.*, **277**, 10813–10823, 2002.

[37] B. Ford, K. Skowronek, S. Boykevisch, D. Bar-Sagi, and N. Nassar, *J. Biol. Chem.*, **280**, 25697–25705, 2005.

[38] Y. Duan, C. Wu, S. Chowdhury, M. C. Lee, W. Xiong, G.and Zhang, R. Yang, P. Cieplak, R. Luo, T. Lee, Caldwell J., J. Wang, and P. Kollman, *J. Comput. Chem.*, **24**, 1999–2012, 2003.

[39] C. L. Foley, L. G. Pedersen, P. S. Charifson, T. A. Darden, A. Wittinghofer, E. F. Pai, and M. W. Andersen, *Biochemistry*, **31**, 4951–4959, 1992.

[40] M. J. Frisch, M. Head-Gordon, H. B. Schlegel, K. Raghavarchi, J. S. Binkley, C. Gonzalez, D. F. Defrees, D. J. Fox, R. A. Whiteside, R. Seeger, C. F. Melius, J. Baker, R. Martin, L. R. Kahn, J. J. P. Stewart, E. M. Fluder, S. Topiol, and J. A. Pople, Gaussian 88, Gaussian Inc. Pittsburg PA 1988.

[41] G. A. Worth, C. Edge, and W. G. Richards, *J. Mol. Model.*, **1**, 123–142, 1995.

[42] L. V. Mello, D. M. F. van Aalten, and J. B. C. Findlay, *Protein Engineering*, **10**, 381–387, 1997.

[43] N. Futatsugi and M. Tsuda, *Biophys. J.*, **81**, 3483–3488, 2001.

[44] C. Kobayashi and S. Saito, *Biophys. J.*, **99**, 3726–3734, 2010.

[45] K. L. Meagher, L. T. Redman, and H. A. Carlson, *J. Comput. Chem.*, **24**, 1016–1025, 2003.

[46] M. J. Frisch, G. W. Trucks, H. B. Schlegel, G. E. Scuseria, M. A. Robb, J. R. Cheeseman, G. Scalmani, V. Barone, B. Mennucci, G. A. Petersson, H. Nakatsuji, M. Caricato, X. Li, H. P. Hratchian, A. F. Izmaylov, J. Bloino, G. Zheng, J. L. Sonnenberg, M. Hada, M. Ehara, K. Toyota, R. Fukuda, J. Hasegawa, M. Ishida, T. Nakajima, Y. Honda, O. Kitao, H. Nakai, T. Vreven, J. A. Montgomery, Jr., J. E. Peralta, F. Ogliaro, M. Bearpark, J. J. Heyd, E. Brothers, K. N. Kudin, V. N. Staroverov, R. Kobayashi, J. Normand, K. Raghavachari, A. Rendell, J. C. Burant, S. S. Iyengar, J. Tomasi, M. Cossi, N. Rega, J. M. Millam, M. Klene, J. E. Knox, J. B. Cross, V. Bakken, C. Adamo, J. Jaramillo, R. Gomperts, R. E. Stratmann, O. Yazyev, A. J. Austin, R. Cammi, C. Pomelli, J. W. Ochterski, R. L. Martin, K. Morokuma, V. G. Zakrzewski, G. A. Voth, P. Salvador, J. J. Dannenberg, S. Dapprich, A. D. Daniels, . Farkas, J. B. Foresman, J. V. Ortiz, J. Cioslowski, and D. J. Fox, Gaussian 09 Revision A.1, Gaussian Inc. Wallingford CT 2009.

[47] U. C. Singh and P. A. Kollman, *J. Comp. Chem.*, **5**, 129–145, 1984.

[48] D. A. Case, T. A. Darden, T. E. Cheatham III, C. L. Simmerling, J. Wang, R. E. Duke, R. Luo, R. C. Walker, W. Zhang, K. M. Merz, B. Roberts, B. Wang, S. Hayik, A. Roitberg, G. Seabra, I. Kolossváry, K. F. Wong, F. Paesani, J. Vanicek, J. Liu, X. Wu, S. R. Brozell, T. Steinbrecher, H. Gohlke, Q. Cai, X. Ye, J. Wang, M.-J. Hsieh, G. Cui, D. R. Roe, D. H. Mathews, M. G. Seetin, C. Sagui, V. Babin, T. Luchko, S. Gusarov, A. Kovalenko, and P. A. Kollman, *AMBER11*, University of California, San Francisco, 2010.

[49] W. L. Jorgensen, J. Chandrasekhar, J. D Madura, R. W. Impey, and M. L. Klein, *J. Chem. Phys.*, **79**, 926–935, 1983.

[50] H. J. C. Berendsen, J. P. M. Postma, W. F. van Gunsteren, A. DiNola, and J. R. Haak, *J. Chem. Phys.*, **81**, 3684–3690, 1984.

[51] F. Shima, Y. Ijiri, S. Muraoka, J. Liao, M. Ye, M. Araki, K. Matsumoto, N. Yamamoto, T. Sugimoto, Y. Yoshikawa, T. Kumasaka, M. Yamamoto, A. Tamura, and T. Kataoka, *J. Biol. Chem.*, **285**, 22696–22705, 2010.

[52] T. Miyakawa, R. Morikawa, M. Takasu, K. Sugimori, K. Kawaguchi, H. Saito, and H. Nagao, accepted for publication in *Progress in Theo-*

retical Chemistry and Physics, 2012.

[53] X. Du, G. E. Black, P. Lecchi, F. P. Abramson, and S. R. Sprang, *Proc. Natl. Acad. Sci. USA*, **101**, 8858, 2004.